

# Structural Organization and Function of Mouse Photoreceptor Ribbon Synapses Involve the Immunoglobulin Protein Synaptic Cell Adhesion Molecule 1

Adema Ribic,<sup>1\*</sup> Xinran Liu,<sup>2</sup> Michael C. Crair,<sup>3</sup> and Thomas Biederer<sup>1\*</sup>

<sup>1</sup>Department of Molecular Biophysics and Biochemistry, Yale University, New Haven, Connecticut 06520-8024 and Department of Neuroscience, Tufts University School of Medicine, Boston, Massachusetts 02111-0081

<sup>2</sup>Department of Cell Biology, Yale University, New Haven, Connecticut 06520-8024

<sup>3</sup>Department of Neurobiology, Yale University, New Haven, Connecticut 06520-8024

## ABSTRACT

Adhesive interactions in the retina instruct the developmental specification of inner retinal layers. However, potential roles of adhesion in the development and function of photoreceptor synapses remain incompletely understood. This contrasts with our understanding of synapse development in the CNS, which can be guided by select adhesion molecules such as the Synaptic Cell Adhesion Molecule 1 (SynCAM 1/CADM1/nectin-like 2 protein). This immunoglobulin superfamily protein modulates the development and plasticity of classical excitatory synapses. We show here by immunoelectron microscopy and immunoblotting that SynCAM 1 is expressed on mouse rod photoreceptors and their terminals in the outer nuclear and plexiform layers in a developmentally regulated manner. Expression of SynCAM 1 on rods is low in early postnatal stages (P3–

P7) but increases after eye opening (P14). In support of functional roles in the photoreceptors, electroretinogram recordings demonstrate impaired responses to light stimulation in SynCAM 1 knockout (KO) mice. In addition, the structural integrity of synapses in the OPL requires SynCAM 1. Quantitative ultrastructural analysis of SynCAM 1 KO retina measured fewer fully assembled, triadic rod ribbon synapses. Furthermore, rod synapse ribbons are shortened in KO mice, and protein levels of Ribeye, a major structural component of ribbons, are reduced in SynCAM 1 KO retina. Together, our results implicate SynCAM 1 in the synaptic organization of the rod visual pathway and provide evidence for novel roles of synaptic adhesion in the structural and functional integrity of ribbon synapses. *J. Comp. Neurol.* 522:900–920, 2014.

© 2013 Wiley Periodicals, Inc.

**INDEXING TERMS:** SynCAM; CADM; nectin-like protein; ribbon synapse; retina; rod; electroretinography

Precise synapse development is crucial for integration of neurons into functional networks. Progress over recent years has implicated different classes of adhesion molecules in these processes (Fuerst and Burgess, 2009; Missler et al., 2012; Shapiro et al., 2007). Among these proteins, cadherin and immunoglobulin (Ig) superfamily members, as well as neurexins and neuroligins, organize the development and maturation of synapses in the CNS. Specifically, the Ig protein Synaptic Cell Adhesion Molecule 1 (SynCAM 1) that is enriched at central synapses of vertebrates promotes the formation of hippocampal excitatory synapses *in vitro* and *in vivo* and contributes to their maintenance (Biederer et al., 2002; Fogel et al., 2007; Robbins et al., 2010).

SynCAM 1 mediates cellular adhesion in a variety of tissues and is most prominently expressed in the brain

(Fogel et al., 2007; Fujita et al., 2007; Thomas et al., 2008; Watabe et al., 2003). SynCAM 1 is enriched at excitatory synapses in the forebrain and instructs their formation in developing hippocampal neurons via adhesive interactions across the synaptic cleft (Biederer et al., 2002; Fogel et al., 2007, 2011; Robbins et al., 2010). It is then required in the maturing hippocampus to maintain

Grant sponsor: Knights Templar Eye Foundation (to A.R.); National Institutes of Health; Grant number: R01 DA018928 (to T.B.); Grant number: P30 EY000785; Grant number: R01 EY015788 (to M.C.C.).

\*CORRESPONDENCE TO: Adema Ribic or Thomas Biederer, Department of Neuroscience, Tufts University School of Medicine, Boston, MA 02111-0081. E-mails: adema.ribic@tufts.edu and thomas.biederer@tufts.edu

Received February 4, 2013; Revised May 23, 2013;

Accepted August 14, 2013.

DOI 10.1002/cne.23452

Published online August 24, 2013 in Wiley Online Library (wileyonlinelibrary.com)

© 2013 Wiley Periodicals, Inc.

**TABLE 1.**  
List of Antibodies

Antibody	Immunogen	Manufacturer and catalog No.	Host species and clonality	Dilution and application
Actin	Amino acids (aa) 18–40 of chicken gizzard Actin	MP Biomedicals, Solon, OH; 08691002; clone C4	Mouse monoclonal	1:8,000 (WB)
Calbindin	Recombinant rat Calbindin D-28k	Swant (Bellinzona, Switzerland); CB-38	Rabbit polyclonal	1:2,000 (IHC)
mGluR6	C-terminus of rat mGluR6 (AAPPQENADAK)	Neuromics, Edina, MN; RA13105	Rabbit polyclonal	1:300 (IHC)
Neurofilament	Semipurified adult Wistar rat neurofilaments	Developmental Studies Hybridoma Bank, University of Iowa; clone RT97	Mouse monoclonal	1:10 (IHC)
PKC $\alpha$	Recombinant human PKC $\alpha$	Cell Signaling Technology, Beverly, MA; 2056	Rabbit polyclonal	1:200 (IHC)
PSD95	N-terminus of human PSD-95 (CDTLEAPGYELQVNGTEGEMEY)	Cell Signaling Technology, Beverly, MA; 3409	Rabbit monoclonal	1:200 (IHC)
Ribeye	Glutathione S-transferase (GST) fusion protein containing aa 563–988 of rat Ribeye (U2656)	Dr. Thomas Südhof; Stanford University School of Medicine, CA (Kindly provided by Dr. Sreeganga Chandra, Yale University, CT)	Rabbit polyclonal	1:1,000 (WB)
Ribeye	Mouse Ribeye C-terminus, aa 361–445	BD Biosciences (San Jose, CA); 612044	Mouse monoclonal	1:500 (IHC)
SynCAM 1	Extracellular domain of SynCAM 1 fused to Fc fragment	MBL Laboratories, Nagoya, Japan; CM004-3; clone 3E1	Chicken monoclonal	1:1,000 (WB, IHC); 1:20 (cryo-EM)
VGlut1	C-terminus of 493–560 of rat VGlut1 (aa 493–560)	NeuroMab, University of California Davis, CA; 75-066; clone N28/9	Mouse monoclonal	1:200 (IHC)

the synapses that it induced during development (Robbins et al., 2010). Roles of synaptic adhesion proteins such as SynCAM 1 in the assembly and function of neuronal circuitry, however, remain to be defined. SynCAM 1 transcripts are abundantly expressed in the retina of different species, including mice, zebrafish, and chick (Fujita et al., 2005; Pietri et al., 2008; Wahlin et al., 2008). Roles of other cell adhesion molecules in retinal development, and particularly in the synaptic specification of inner retinal layers, have been well described (Fuerst et al., 2009; Fuerst and Burgess, 2009; Lefebvre et al., 2008; Yamagata and Sanes, 2008). However, the localization and function of SynCAM 1 in this part of the CNS have not yet been investigated in detail.

Here we address the contributions of SynCAM 1 to retinal synaptic organization and function. Analyzing mice lacking SynCAM 1, our results demonstrate that this protein contributes to organizing the structure and molecular composition of photoreceptor synapses. Specifically, the ultrastructure of synaptic ribbons was altered and the content of the major ribbon protein Ribeye was reduced upon loss of SynCAM 1. Furthermore, SynCAM 1 knockout (KO) mice have fewer fully assembled, mature ribbon synapses. On a functional level, we show SynCAM 1 to be necessary for rod-, but not cone-, mediated visual transduction and SynCAM 1 KO mice have altered retinal network activity. These findings provide novel insights into the roles of synaptic adhesion in the organization of ribbon synapses and retinal circuits.

## MATERIALS AND METHODS

### Animals

Experiments were performed on C57BL6/J wild-type (WT) mice (The Jackson Laboratory, Bar Harbor, ME), SynCAM 1 KO mice (Fujita et al., 2006), and their WT littermates. SynCAM 1 KO mice had been back-crossed for at least 10 generations and were maintained on a C57BL6/J background. Animals of both sexes from postnatal day 3 (P3) to P50 were used for all experiments, as indicated below and stated in the figure legends. SynCAM 1 KO and WT littermates were compared in all experiments, and experimenters were blind to the genotype of animals used. Animals were kept on a 12/12-hour light/dark cycle with food and water ad libitum. All experiments were performed during the light phase (7:00 AM to 7:00 PM). Animals were treated in accordance with the Yale Institutional Animal Care and Use Committee guidelines.

### Characterization of antibodies and other reagents

Antibodies used, their properties, and their working concentrations are listed in Table 1. Antibody characterization for this study is described below.

### Actin

Mouse anti-Actin monoclonal antibody was raised against amino acids 18–40 of chicken gizzard Actin which is a highly conserved region of the molecule (MP

Biomedicals, Solon, OH; catalog No. 69100; clone C4). Immunoblots demonstrated specificity directed toward Actin across species (manufacturer's data sheet).

### **Calbindin**

Rabbit anti-Calbindin D-28k polyclonal antibody was raised against recombinant rat Calbindin D-28k (Swant, Bellinzona, Switzerland; catalog No. CB-38; lot 9.03). Immunoblotting recognizes a single band of approximately 28 kDa, and the antibody does not stain the brain of Calbindin D-28k KO mice (manufacturer's data sheet). The staining pattern of this antibody in our study is consistent with previously published results (Hirano et al., 2011).

### **mGluR6**

Rabbit anti-mGluR6 polyclonal antibody was raised against rat mGluR6 C-terminal sequence AAPPQNENADAK (Neuromics, Edina, MN; catalog No. RA13105). Immunoblotting recognizes a band of approximately 97 kDa (manufacturer's data sheet). As a control, we used preincubation with immunizing peptide (Neuromics; catalog No. P13105), which abolished all signal in retinal sections of WT mice. Although this antibody in our hands did not result in punctate staining (tom Dieck et al., 2012), the staining pattern obtained was almost identical to that in previously published studies using different antibodies (Cooper et al., 2012).

### **Neurofilament**

Mouse anti-Neurofilament monoclonal antibody was raised against semipurified adult Wistar rat neurofilaments (Developmental Studies Hybridoma Bank, University of Iowa; clone RT97). The staining pattern of this antibody in our study is consistent with that in previously published studies using different antibodies (Haverkamp and Wässle, 2000).

### **PKC $\alpha$**

Rabbit anti-protein kinase C  $\alpha$  polyclonal antibody was raised against recombinant human PKC $\alpha$  (Cell Signaling Technology, Beverly, MA; catalog No. 2056). Immunoblotting detects a single band at approximately 80 kDa, and the antibody does not cross-react with other PKC isoforms (manufacturer's data sheet). The staining pattern of this antibody in our study is consistent with that in previously published studies using different antibodies against PKC $\alpha$  (Haverkamp and Wässle, 2000).

### **PNA**

PNA-biotin conjugate (peanut lectin agglutinin, biotin conjugate; Sigma, St. Louis, MO; catalog No. L6135) was used at a final concentration of 5  $\mu$ g/ml and rec-

ognized cone terminals in the outer plexiform layer (OPL) as previously described (Reim et al., 2009).

### **PSD-95**

Rabbit anti-postsynaptic density protein of 95 kDa (PSD-95) monoclonal antibody was raised against synthetic peptide corresponding to the N-terminal human PSD-95 sequence CDTLEAPGYELQVNGTEGEMEY (Cell Signaling Technology, Beverly, MA; catalog No. 3409). Immunoblotting recognizes a single band at approximately 95 kDa, and the tissue staining is abolished in the presence of control peptide (manufacturer's data sheet). This antibody gave a staining pattern identical to that in previously published studies using different antibodies against PSD-95 (Yang et al., 2007).

### **Ribeye**

Rabbit polyclonal antibody against Ribeye (kindly provided by Sreeranga Chandra, Yale University) used in immunoblotting was raised against glutathione S-transferase (GST) fusion protein containing amino acids 563–988 of rat Ribeye (U2656) as previously described (Schmitz et al., 2000). In our study, this antibody recognized a prominent band of approximately 120 kDa in retinal protein extracts and a weaker band corresponding to CtBP2 at about 50 kDa, as previously described (Schmitz et al., 2000). Because of high background that this antibody gave in immunohistology, we used a commercially available mouse monoclonal antibody against Ribeye raised against amino acids 361–445 in Ribeye C-terminus (BD Biosciences, San Jose, CA; catalog No. 612044). Staining with this antibody detected typical horseshoe-shaped ribbons in the OPL as described by Wahlin et al. (2010).

### **SynCAM 1**

Anti-SynCAM 1 antibody was purified from hybridoma supernatant using anti-IgY affinity column (MBL Laboratories, Nagoya, Japan; CM004-3; clone 3E1). This hybridoma was established by fusion of chicken B cell line MUH1 cell with chicken splenocyte immunized with recombinant extracellular domain of SynCAM 1 fused to Fc fragment (manufacturer's data sheet). This antibody was extensively tested in our laboratory in various applications. In immunoblotting with retinal tissue homogenates, this antibody detected multiple bands around 100 kDa in WT samples as a result of the complex N-glycosylation of this protein (Fig. 1; Fogel et al., 2007). No bands were observed in SynCAM 1 KO samples (Fig. 1). Additionally, this antibody stained SynCAM 1 throughout the WT retina, whereas almost no staining was observed in SynCAM 1 KO retinas (Fig. 1).

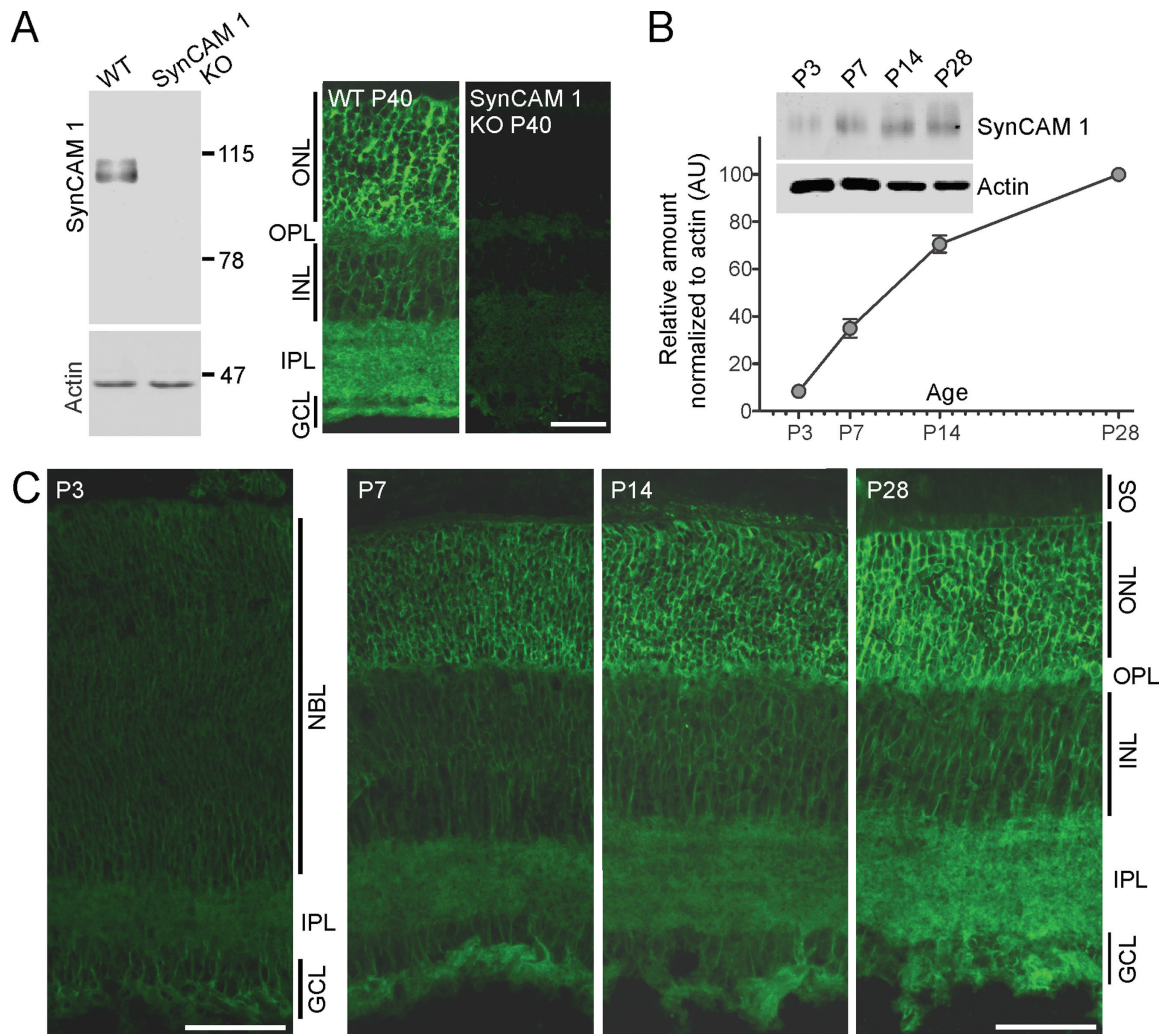


**Figure 1.** Expression of SynCAM 1 in the retina is developmentally regulated. **A:** Left: SynCAM 1 is detected as multiple bands around 100 kDa in the retina, indicating a similar extent of glycan modifications as in hippocampus (Fogel et al., 2007). SynCAM 1 KO retina served as specificity control for the antibody. Actin was used as a loading control. Molecular weights are indicated in kilodaltons. Right: Maximum-intensity projection of SynCAM 1 labeling throughout the adult mouse retina (P40) measured its prominent expression in outer nuclear and plexiform layers. Only low background staining was detected in SynCAM 1 KO. **B:** Top: Expression of SynCAM 1 progressively increased during retinal development as detected by quantitative immunoblotting, starting to be detectable at P3 and steadily rising through P28. Bottom: Quantification of immunoblots shows a steady increase in SynCAM 1 expression during development of retina. Data are represented as mean  $\pm$  SEM of three independent experiments.  $N = 2$  animals/age point. **C:** Gradual increase of SynCAM 1 expression was evident in immunohistochemistry. SynCAM 1 is initially expressed at low levels in all developing layers (P3). At P7, expression starts to be more detectable in the ONL. SynCAM 1 already appears enriched in ONL and OPL at P14, with a high expression level at P28. All images are maximum-intensity projections of Z-stacks through central retina. ONL, outer nuclear layer; OPL, outer plexiform layer; INL, inner nuclear layer; IPL, inner plexiform layer; GCL, ganglion cell layer; OS, outer segments; NBL, neuroblast layer; P, postnatal day. Scale bars = 30  $\mu$ m in A; 50  $\mu$ m in C.

### VGlut1

Anti-vesicular glutamate transporter 1 (VGLUT1) mouse monoclonal antibody was produced against the cytoplasmic C-terminus of rat VGLUT1 (amino acids 493–560; NeuroMab, UC Davis, CA; catalog No. 75-066; clone N28/9). Immunoblotting recognizes a single band of approximately 52 kDa with adult rat brain homogenates (manufacturer's data sheet). The labeling that we

detected with this antibody was identical to that in previously published studies (Sherry et al., 2003).

### Secondary antibodies

For all immunostainings, secondary antibodies were applied in the absence of primary antibodies as a control. The following secondary antibodies were used for immunofluorescence: anti-chicken Alexa 488, anti-rabbit

Alexa 488 (Invitrogen Life Technologies, Grand Island, NY), and anti-rabbit and anti-mouse Cy3 (1:1,000; Jackson ImmunoResearch, West Grove, PA). PNA-biotin was detected with streptavidin-Alexa 555 (1:1,000; Invitrogen Life Technologies). For electron microscopy, secondary donkey anti-chicken 12-nm gold conjugate (Jackson ImmunoResearch) was used. For quantitative immunoblotting, secondary IRDye800 antibodies were used at 1:4,000 (Rockland Immunochemicals, Gilbertsville, PA).

### Tissue preparation for biochemistry and microscopy

Animals were anesthetized with ketamine (100 mg/kg) and xylazine (10 mg/kg) in saline. For all experiments (except for those depicted in Fig. 1), animals were dark adapted overnight, and all procedures were performed under dim red light (scotopic conditions). For protein isolation (animals aged P3–P28 for Fig. 1, P35–P50 for Fig. 8), cornea was cut with a sterile blade, and the lens was gently squeezed out of the eye with fine forceps. The retina was isolated by gently squeezing the eyecup with fine forceps after clearing out the vitreous fluid and immediately frozen over dry ice, followed by sonication in 8 M urea. Protein concentrations were determined by using the BCA method (Thermo-Fisher Scientific, Holtsville, NY). For microscopy, animals (P3–P50, as indicated in figure legends) were transcardially perfused first with ice-cold phosphate-buffered saline (PBS) and then with either 4% paraformaldehyde (PFA; in PBS, pH 7.4) for tissues to be used in light microscopy or with Karnovsky's fixative (Karnovsky, 1964) for electron microscopy. For light microscopy, whole eyes were postfixed for 1 hour in 4% PFA and washed in PBS overnight at 4°C. Isolated eyecups were cryoprotected in 30% sucrose in PBS prior to embedding in OCT (Tissue-Tek; Sakura Finetek, Torrance, CA). Tissue was sectioned on a cryotome (Leica Nussloch, Germany) at a thickness of 15  $\mu$ m and directly mounted on Superfrost Plus slides (EMS, Hatfield, PA). For all experiments, eyecups from all animals to be used were embedded together in a series in order to process them in the same way.

For electron microscopy, tissue was first postfixed in Karnovsky's fixative for 1 hour at 4°C and then washed in 0.1 M sodium-cacodylate. Central retina was dissected under a microscope before osmication in Palade's osmium (Palade, 1952). Tissue was then dehydrated through graded series of ethanol and propylene oxide and embedded in EMBed-812 resin (EMS) before cutting on a Leica Ultracut UTC microtome at 70-nm thickness. The sections were then placed on

200-mesh formvar/carbon coated copper grids and stained with 2% aqueous uranyl acetate (UA) and lead citrate.

For immunoelectron microscopy, samples were fixed after perfusion in 4% paraformaldehyde/0.1% glutaraldehyde in PBS for 15 minutes and then with 4% PFA in PBS for 1 hour. Samples were cryoprotected in 2.3 M sucrose overnight at 4°C. These were then rapidly frozen onto aluminum pins in liquid nitrogen. The frozen block of tissue was trimmed on a Leica Cryo-EMUC6 UltraCut, and 60-nm-thick sections were collected using the Tokuyasu (1973) method. The frozen sections were thawed and placed on a nickel formvar/carbon-coated grid floating in a dish of PBS, ready for immunolabeling.

### Immunolabeling of sections for electron microscopy

Grids were placed section side downward on drops of 0.1 M ammonium chloride for 10 minutes to quench untreated aldehyde groups, then blocked for nonspecific binding in PBS buffer containing 1% bovine serum albumin (BSA; Sigma) and 10% normal donkey serum (Jackson ImmunoResearch) for 20 minutes. They were then incubated in primary chicken anti-SynCAM 1 (MBL; described above) for 30 minutes. Rinsed grids were placed in secondary donkey anti-chicken 12-nm gold conjugate (Jackson ImmunoResearch) for 30 minutes, rinsed in PBS, fixed using 1% glutaraldehyde, rinsed in distilled water, and transferred to a UA/methylcellulose drop for 10 minutes. Samples were viewed on an FEI Tecnai Biotwin TEM (FEI, Hillsboro, OR) at 80 kV. Images were taken with a Morada CCD and iTEM (Olympus) software. Acquired images were imported into ImageJ (NIH), and immunogold distribution was analyzed using the multipoint selection tool.

### Retinal morphology and electron microscopy

For estimating the density of photoreceptor nuclei, we employed the disector method (Li and Cline, 2010; Sterio, 1984; Yen et al., 1993). Osmicated and dehydrated tissue from central retina (see above) was cut on a Leica Ultracut UTC microtome at 0.5  $\mu$ m and stained with toluidine blue. At minimum three series of five pairs of adjacent sections (5  $\mu$ m apart, to avoid sampling the same nuclei) were imaged per animal (three animals per group). Images were acquired with a Zeiss AxioImager Z2 microscope and AxioVision Software (Zeiss). Images were imported into ImageJ and scaled, and layer thickness was measured by drawing straight lines on random locations throughout the sections with the line tool in ImageJ. Photoreceptor count was performed on the same images manually using the

Cell Counter plugin in ImageJ following the rules of the disector method (in each chosen area, only nuclei that appeared in the reference section, but not in the look-up section, were counted; Li and Cline, 2010; Sterio, 1984; Yen et al., 1993). All measurements were averaged per animal before performing statistical comparisons.

For electron microscopy, images were acquired with a Zeiss 910 electron microscope. Series of 70-nm ultra-thin sections (see above) were sampled for the disector analysis (Li and Cline, 2010; Sterio, 1984; Yen et al., 1993). Sections were 3  $\mu\text{m}$  apart to avoid sampling the same terminals in the OPL. Six pairs of adjacent sections in a series (minimum three series per animal, three animals per group) were imaged for analysis at  $\times 16,000$  using Kodak Electron Microscope film 4489. Films were then scanned at high resolution with an Epson Perfection 4990 PHOTO scanner. To ensure equal sampling, all samples were treated in an identical manner. The majority of triad images acquired had arciform density present, as well as similar overall appearance of the presynaptic ribbon complex, confirming that all images were acquired from comparable planes of sectioning. Rods and cones were distinguished on the basis of previously published criteria (Carter-Dawson and LaVail, 1979). Digital images were imported and scaled in ImageJ, and all analyses were performed with ImageJ. Terminal perimeter was measured only for terminals with entire cross-section profile in the acquired image. Synaptic vesicles were counted manually with multipoint selection in ImageJ. Terminal perimeter and perimeter of horizontal and bipolar cell processes were measured with the freehand tool in ImageJ. Synaptic ribbon height was measured with the segmented line tool in ImageJ. Triad and ribbon density and terminal density were counted manually using the disector method (Li and Cline, 2010; Sterio, 1984; Yen et al., 1993). All measurements were averaged per animal before performing statistical analysis. Representative micrographs were imported in CorelDraw X5 (Corel Inc., Mountain View, CA) and trace outlined to make relevant structures readily visible.

### Immunohistochemistry and confocal microscopy

Primary antibodies used in double-labeling experiments were applied simultaneously, and blocking steps were performed with normal serum of the host species from which the secondary antibodies had been derived. Sections were encircled with Pap-Pen (Sigma), and non-specific antibody binding sites were blocked with 3% normal serum and 0.03% Triton X-100 (Sigma) in PBS

for 1 hour in a humid chamber. Primary and secondary antibodies were diluted in 3% normal serum and 0.03% Triton X-100 in PBS and incubated for either 1 hour at room temperature or overnight at 4°C. After the antibody incubation steps, sections were washed in PBS and in distilled water before coverslipping with mounting medium (Aqua-Polymount; Polysciences, Warrington, PA). Confocal microscopy was performed with a laser scanning microscope (LSM 710 and LSM 510; Zeiss, Jena, Germany) with argon (488 nm) and helium/neon (543 nm) lasers. For image acquisition of SynCAM 1 and DAPI, an FV10i (Olympus, Tokyo, Japan) with  $\times 60$  silicone oil objective ( $\text{NA}_{\text{objective}} = 1.35$ ;  $\text{NA}_{\text{oil}} = 1.406$ ; Olympus) was used, and settings were kept similar to those of the LSM 510/710. Image acquisition for all images was performed in multiple-tracking mode. High-magnification images of central retina (except as noted above) were obtained at a resolution of  $1,024 \times 1,024$  or  $2,048 \times 2,048$  pixels using a Zeiss EC Plan-Neofluar  $\times 40$  air (NA = 0.75; Fig. 1) or Zeiss Apochromat  $\times 63$  oil objective (NA = 1.4; all other experiments) and immersion oil (Immersionol, Zeiss; refractive index = 1.518). Pinholes for both lasers were kept such that all optical sections were of the same thickness (0.8  $\mu\text{m}$ ). For colocalization, regions of interest were acquired mainly as single optical sections. For developmental profiling of Calbindin immunoreactivity, acquisition settings were kept equal for all samples and were such to allow for detection of horizontal cell sprouting in the ONL. For Ribeye analysis,  $50 \times 25 \mu\text{m}$  Z-stacks (at  $2,048 \times 1,024$  pixels) were taken at random locations throughout the OPL at 0.43- $\mu\text{m}$  intervals. They were later analyzed in ImageJ with the freehand and multipoint tools to label and measure their length and number. For length measurements, approximately 500 ribbons per animal were analyzed. For number measurements, we employed the optical disector technique (Jinno et al., 1998; West et al., 1991). For all experimental groups (N = 2–3 animals per genotype per age), all imaging settings (laser power, gain, and offset) were kept identical. Images were minimally corrected for brightness and contrast (in identical manner for all groups) using the Zen software program (Zeiss) and assembled in CorelDraw X5.

### Quantitative immunoblotting

Proteins from retinal homogenates (30  $\mu\text{g}$ , prepared as described above) were subjected to immunoblotting using standard procedures (Fogel et al., 2007) and scanned with the Odyssey Infrared Imaging System (Li-Cor Biosciences, Lincoln, NE). Quantification was performed with the gel analysis plugin in ImageJ, with Actin as loading control for all samples.

## Electroretinogram recordings

Electroretinogram (ERG) recordings were performed as previously described (Vistamehr and Tian, 2004). Briefly, for scotopic responses, animals (P35–P50) were dark adapted overnight and anesthetized with ketamine and xylazine as described above. The pupils were dilated with 1% atropine (Sigma) and 2.5% phenylephrine HCl (TCI, Portland, OR), and the corneal surface was protected with 0.5% methylcellulose (Bausch & Lomb, Rochester, NY). ERGs were evoked by LED-generated white-light flashes (less than 5 msec in duration; BigShot Ganzfeld; LKC Technologies, Gaithersburg, MD) and recorded with circular corneal platinum custom-made electrodes. Signals were amplified and bandpass filtered between 0.3 and 500 Hz. For rod responses, ERGs for each light intensity were averaged from five consecutive flashes with 30-second interstimulus recovery periods. Light intensities delivered were in 5-dB steps ranging from  $-25$  dB to 10 dB, where 0 dB =  $2.5$  cd/m<sup>2</sup>. Double-flash recordings were performed as previously described (Kim et al., 2005), and signals were averaged from three consecutive stimuli with a 2-minute recovery period between. For photopic ERGs, animals were light adapted, and signals for each light intensity ( $-5$  dB to 10 dB in 5-dB steps) were averaged from 10 consecutive flashes delivered at a frequency of 2 Hz. Traces were analyzed with EMWin (LKC Technologies). a-wave and b-wave amplitude and latency were measured after removing the oscillatory potentials, where a-wave was measured from baseline to the trough, and b-wave was measured from the trough of the a-wave to the peak of the b-wave. a- and b-wave time was measured from the time of the flash to a-wave trough and b-wave peak, respectively. Amplitude and latency of oscillatory potentials were measured using automatic finite impulse response high-pass filtering function of EMWin with a corner frequency set at 75 Hz (LKC Technologies). Amplitude of oscillatory potential peaks was automatically analyzed with EMWin after filtering and is a sum of OP1–5 amplitudes. Latency was analyzed manually after filtering, where OP1 and OP5 were not evaluated because of their small amplitude (Vessey et al., 2012). For double-flash recordings, only the a-wave was measured. For double-flash recordings, amplitude of the probe flash a-wave normalized to test flash a-wave was plotted in relation to the time between the two flashes and fit using the second-order polynomial equation in GraphPad Prism 4.0 (GraphPad Inc., La Jolla, CA).

## Data analysis

All quantitated analyses were performed with the researchers blind to the condition. Statistical analyses were performed in GraphPad Prism 4.0 with Student's

*t*-test, two-way ANOVA, or two-way repeated measures (RM) ANOVA (as indicated in text and figure legends) unless stated otherwise. All data are reported as mean  $\pm$  SEM.

## RESULTS

### Expression of retinal SynCAM 1 is developmentally regulated

We quantified the expression of SynCAM 1 protein during the main stages of mouse retinal development using a commercial antibody that specifically recognized SynCAM 1 in retinal homogenates and in immunohistochemistry (Fig. 1A; Fogel et al., 2011). This antibody detected multiple bands of approximately 100 kDa in Western blots of total retinal homogenates from WT mice (Fig. 1A, left), likely corresponding to different glycosylation forms of SynCAM 1 (Fogel et al., 2007). No bands were detected in samples from SynCAM 1 KO mice (Fig. 1A, left). Additionally, SynCAM 1 protein was specifically detected via immunohistochemistry throughout the WT adult mouse retina (Fig. 1A, right).

The increase of SynCAM 1 protein levels in the retina closely followed the rates of synaptogenesis in this brain region (Fisher, 1979; Regus-Leidig et al., 2009; Sharma et al., 2003), being low early in postnatal development (P3), increasing at P7, and rising after eye opening (P14 and P28; Fig. 1B,C). Similar expression level changes were observed from immunohistochemistry, which showed that SynCAM 1 was expressed at low amounts throughout the retina at P3 and steadily increased during later stages (P7–P28; Fig. 1C). SynCAM 1 signal appeared particularly enriched in the outer nuclear layer (ONL) surrounding photoreceptor cell bodies as well as in the OPL on the photoreceptor terminals (Fig. 1A,C; see also Fig. 2A,D). Despite its abundance in the ONL and OPL, SynCAM 1 was almost undetectable in the photoreceptor inner and outer segments (IS and OS; Fig. 1C and data not shown). SynCAM 1 was present in the inner retinal layers as well, but appeared not to be as abundant as in the ONL.

### SynCAM 1 is localized to photoreceptor cell bodies and terminal membranes in the ONL and OPL

The membrane protein SynCAM 1 localizes to cellular adhesion sites in different systems (Fogel et al., 2007; Watabe et al., 2003). In agreement, immunostaining and cryoimmunoelectron microscopy (EM) demonstrated the presence of SynCAM 1 at the contact points between photoreceptor cell bodies (Fig. 2A,B). Analysis of the distribution of gold particles showed that they localize predominantly to the photoreceptor

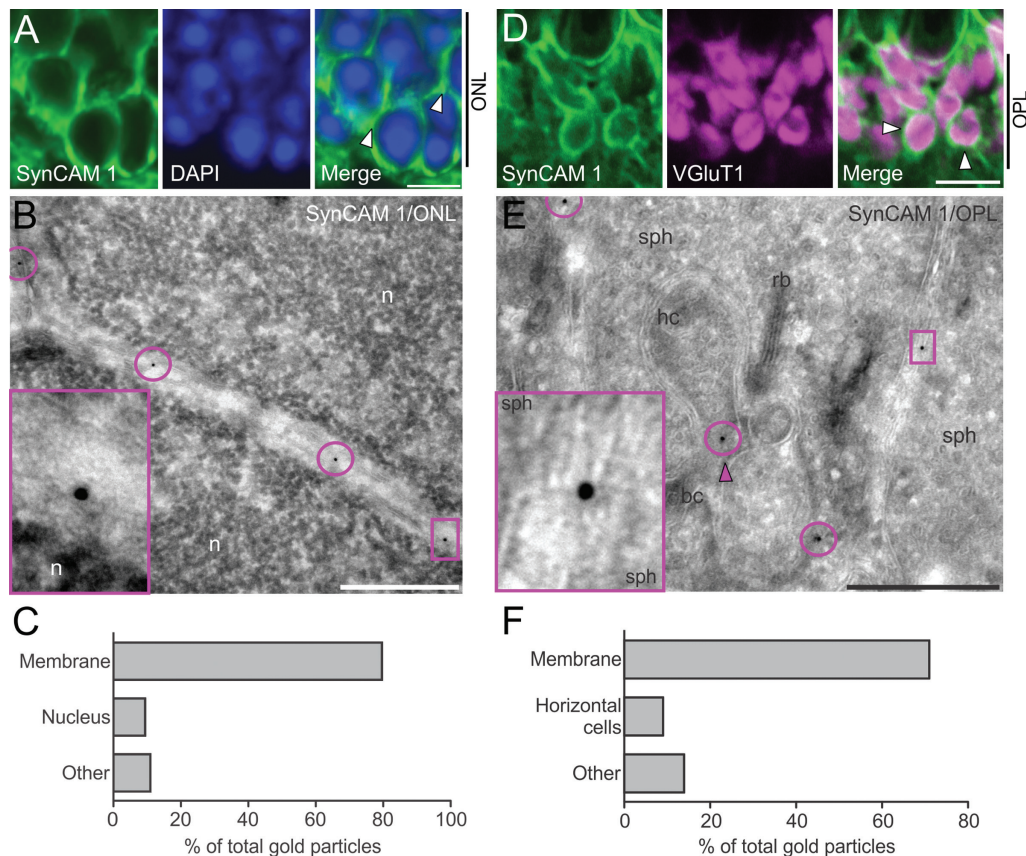


**Figure 2.** SynCAM 1 is localized on photoreceptor cell bodies and surrounds terminal membranes. **A:** SynCAM 1 (green) in the ONL envelops DAPI-labeled photoreceptor nuclei (arrowheads in merged channel) in P40 mouse retina. **B:** Immunoelectron microscopy demonstrated an even distribution of SynCAM 1 at the photoreceptor cell body membrane (circles) in P42 mouse retina. **Inset** depicts enlarged SynCAM 1-immunogold localization from the boxed area. **C:** Distribution of SynCAM 1-immunogold label (percentage) in different subregions of photoreceptor cell bodies in the ONL (total of 220 gold particles counted on 47 photoreceptor cell bodies; see text for details). **D:** SynCAM 1 (green) is expressed in OPL, where it encircles VGlut1-positive photoreceptor terminals (magenta) in P40 mouse retina (arrowheads in merged image). **E:** Immunoelectron microscopy demonstrated the presence of SynCAM 1 at the membrane of photoreceptor terminals (circles) as well as at the interface of photoreceptor terminal with a horizontal cell process (arrowhead) in P42 mouse retina. **Inset** depicts enlarged SynCAM 1-immunogold localization from the boxed area. **F:** Distribution of SynCAM 1-immunogold label in different subregions of rod ribbon complex (total of 303 gold particles counted on 106 rod terminals in the OPL; see text for details). ONL, outer nuclear layer; n, nucleus; OPL, outer plexiform layer; sph, spherule, rb, ribbon; hc, horizontal cell; bc, bipolar cell. Scale bars = 10  $\mu$ m in A; 500 nm in B,E; 3  $\mu$ m in D.

plasma membrane in the ONL (80% of  $N = 220$  particles found on  $N = 47$  photoreceptor cell bodies; Fig. 2C), in agreement with our findings at the light microscopic level (Fig. 2A). Gold particles were almost completely absent in SynCAM 1 KO mouse control samples ( $N = 20$  particles on  $N = 42$  photoreceptor cell bodies; data not shown).

SynCAM 1 in the brain is enriched at excitatory synapses and mediates their structural and functional development in the hippocampus (Fogel et al., 2011; Robbins et al., 2010; Shu et al., 2011). Because our results in Figure 1 demonstrated robust SynCAM 1 expression in the outer retinal synaptic layer, we examined whether it is associated with photoreceptor synapses. Photoreceptors connect with their bipolar cell

targets within the OPL through glutamatergic ribbon synapses, specialized for tonic release (Heidelberger et al., 2005; Sterling and Matthews, 2005; tom Dieck and Brandstätter, 2006). Photoreceptor terminals, bipolar cell dendrites, and horizontal cell processes form a triadic synapse in the OPL at whose interface is the ribbon, an electron-dense structure involved in vesicle release at the photoreceptor terminal (Fig. 2D; see also Fig. 7A; Snellman et al., 2011; tom Dieck and Brandstätter, 2006). Photoreceptor terminals (both rod and cone) are specifically labeled with antibodies against VGlut1 (Johnson et al., 2003; Sherry et al., 2003) and were detected as dense clusters of VGlut1 immunoreactivity in the OPL (Fig. 2D). Interestingly, SynCAM 1 signal appeared to envelop the VGlut1

clusters (Fig. 2D; merged image), indicating its presence on the photoreceptor terminal membrane. We have not observed SynCAM 1 signal associated with Calbindin-labeled horizontal cell processes or PKC $\alpha$ -labeled bipolar cell processes in the OPL (data not shown). Immuno-EM analysis confirmed the presence of SynCAM 1 at plasma membrane areas along the rod terminal (Fig. 2E,F; 71% of N = 303 particles found on 106 terminals) as well as at the contact sites between rods and horizontal cell processes (Fig. 2E,F, arrowhead; 9% of N = 303 particles). SynCAM 1 was not detected at the synaptic ribbon complex, but we have occasionally observed gold particles at or near the membrane of horizontal cell processes (Fig. 2E,F). SynCAM 1 was never detected near the ribbons or close to bipolar cell dendrites, nor did we detect SynCAM 1 on Müller cell processes in the outer retina (data not shown). In addition, the few cone terminals we found in our sections (identified by criteria described in Materials and Methods) were labeled very sparsely with SynCAM 1 antibody compared with rod terminals (data not shown). We also detected no SynCAM 1 signal in the photoreceptor IS and OS (data not shown). Specificity of labeling was confirmed in SynCAM 1 KO samples, in which a low number of gold particles could be detected, but they were never present at plasma membrane areas along rod terminals (N = 45 gold particles found on 61 terminals; data not shown).

### Loss of SynCAM 1 affects photoreceptor function

The robust expression of SynCAM 1 in the outer retinal layers and its ultrastructural localization on rod terminals suggested a possible role in the function of photoreceptors. To investigate how the lack of SynCAM 1 affects photoreceptor function, we performed ERG recordings on SynCAM 1 KO mice. ERGs are a robust measure of photoreceptor integrity (a-wave), bipolar cell responses (b-wave), and the activity of inner retina (oscillatory potentials; Kueng-Hitz et al., 1999; Pinto et al., 2007; Weymouth and Vingrys, 2008). ERG recordings were performed on dark-adapted mice to monitor rod activity. Scotopic (rod) response of SynCAM 1 KO mice showed all typical components (Fig. 3A). However, the a-wave of SynCAM 1 KO mice had significantly higher amplitude compared with that of WT mice at all light intensities (Fig. 3B). The a-wave time-to-peak appeared unaltered in KO (Fig. 3D, bottom), and the a-wave in standard ERGs has a substantial photoreceptor contribution (Brown and Watanabe, 1962a,b; Brown et al., 1965). Impairments in the a-wave amplitude such as those observed in SynCAM 1 KO mice are

hence considered to stem mainly from a dysfunction of the photoreceptors (Peachey and Ball, 2003).

The amplitude of bipolar cell response (b-wave) seemed intact in SynCAM 1 KO mice (Fig. 3C), but the time required for the b-wave to reach its peak was significantly prolonged in SynCAM 1 KO mice at almost all light intensities (Fig. 3D, top). Amplitude of oscillatory potentials was also normal in KO mice (Fig. 3E,F). We analyzed the latency of oscillatory potentials and found no differences between WT and KO mice, even at light intensities at which the b-wave had the most pronounced delay ( $tOP_{3WT} = 45.6 \pm 1.2$  msec,  $tOP_{3KO} = 44.5 \pm 0.88$  msec at  $0.791$  cd/m<sup>2</sup>; N = 12 WT and 10 KO; and data not shown). This indicated intact gross inner retinal activity in SynCAM 1 KO mice.

To investigate whether the visual transduction pathway is impaired in SynCAM 1 KO photoreceptors, we performed double-flash ERG recordings (Lyubarsky and Pugh, 1996). This method monitors recovery of photoreceptor currents generated in the OSs after a saturating flash of light, and several studies have shown defects in the kinetics of current recovery in mice carrying mutations in visual transduction pathway proteins (Howes et al., 2002; Song et al., 2011; Zhang et al., 2007). The normalized a-wave recovery amplitude in SynCAM 1 KO mice was not different from that in WT mice (Fig. 3G,H), indicating intact phototransduction in SynCAM 1 KO mice.

Although ERG recordings were obtained from dark-adapted mice to measure rod activity more selectively, responses are nonetheless mixed because of the overlap in wavelength sensitivity of mouse rods and cones (Abd-El-Barr et al., 2009; Ekesten et al., 1998). Therefore, we measured photopic responses in SynCAM 1 KO mice. The photopic ERG reflects mainly the cone response, because the animals are light adapted and all recordings are performed in the presence of rod-saturating background light (Duncan et al., 2006). The photopic b-wave of SynCAM 1 KO mice appeared intact at all light intensities (Fig. 4A), with no difference in amplitude (Fig. 4B) or time-to-peak (Fig. 4C) compared with WT mice. In addition, no differences were detected in the amplitude and timing of photopic a-wave (data not shown). Together, these results support the idea that SynCAM 1 contributes to the transduction of visual stimuli selectively in the retinal rod pathway.

### Loss of SynCAM 1 causes distinct alterations of retinal structure

The temporal expression profile of SynCAM 1 in the retina (Fig. 1B,C) tracks the development of outer retinal layers (Fisher, 1979; Johnson et al., 2003; Sharma

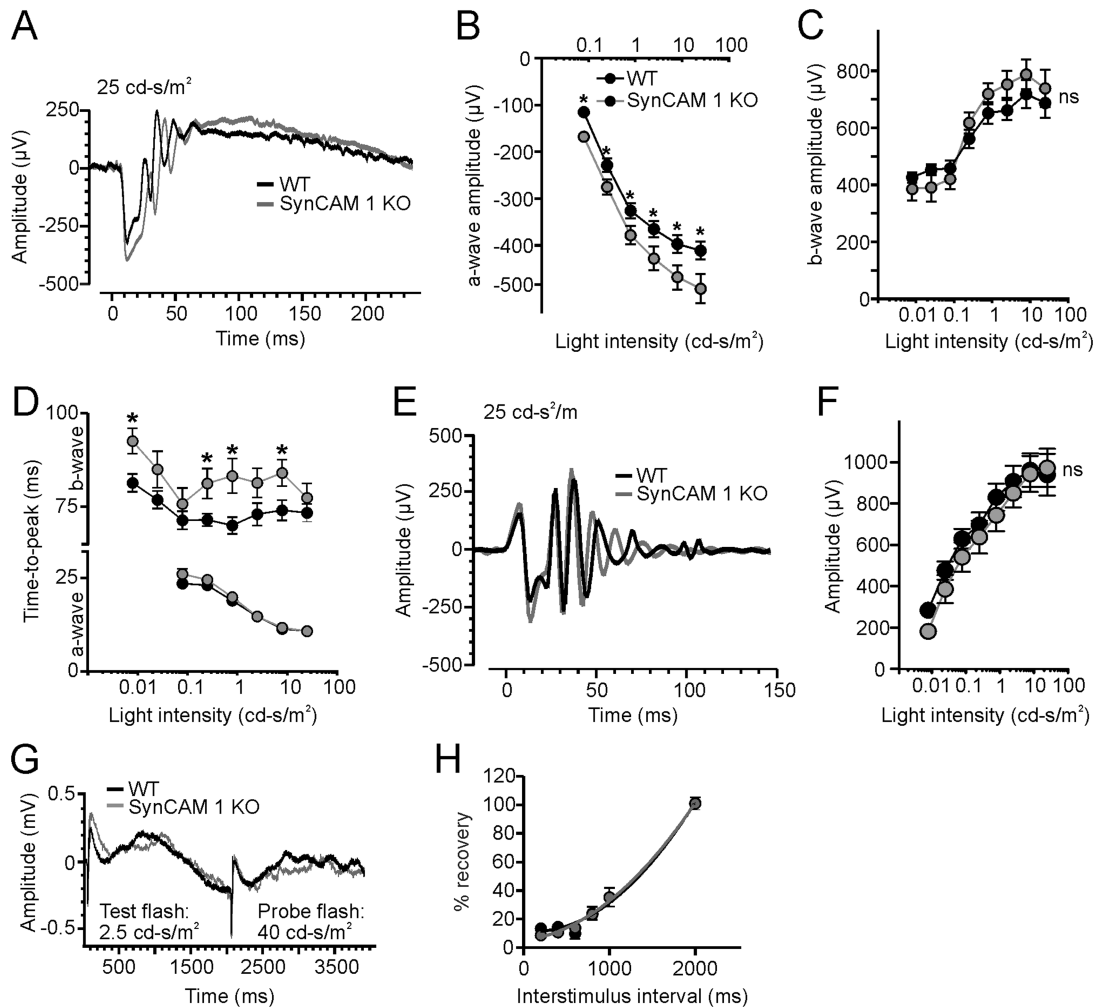


**Figure 3.** Transmission of visual signals is impaired in SynCAM 1 KO retina. **A:** Representative original scotopic ERG traces from SynCAM 1 KO and WT mice (5–7 weeks old) recorded at the highest light intensity used ( $25 \text{ cd}^{-\text{s}}/\text{m}^2$ ). **B:** Rod response was significantly increased in KO mice upon light stimulation. Differences between groups were analyzed by two-way RM ANOVA with post hoc Holm-Sidak comparison. No interaction was found between light intensity and genotype ( $F_{5,100} = 0.78$ ,  $P = 0.56$ ). Effects of genotype on amplitude of light responses were significantly altered:  $F_{1,100} = 6.90$ ,  $*P = 0.016$ .  $N = 12$  WT and 10 KO, age: P40–P50. **C:** Bipolar cell responses are normal in amplitude in KO mice across all light intensities. Differences between groups were analyzed by two-way RM ANOVA: ns, not significant.  $N = 12$  WT and 10 KO. **D:** Top: b-Wave time-to-peak is mildly, but significantly, delayed in KO mice. No interaction was found between light intensity and genotype ( $F_{7,140} = 1.34$ ,  $P = 0.23$ ). Effects of genotype on time-to-peak of light responses were significantly altered ( $F_{1,140} = 5.25$ ,  $*P = 0.033$ ). Bottom: a-Wave time-to-peak is not significantly changed in KO mice. Differences between groups were analyzed by two-way RM ANOVA.  $N = 12$  WT and 10 KO. **E:** Representative oscillatory potentials extracted from ERGs of SynCAM 1 KO and WT mice recorded at the highest light intensity used ( $25 \text{ cd}^{-\text{s}}/\text{m}^2$ ). **F:** Amplitude of oscillatory potentials is intact in SynCAM 1 KO mice. Differences between groups were analyzed by two-way RM ANOVA: ns, not significant.  $N = 12$  WT and 10 KO. **G:** Representative original traces of double-flash ERG recordings obtained from WT and KO mice at light intensities indicated. Interstimulus interval was 1,600 msec. **H:** Recovery of a-wave amplitude as a function of interstimulus interval. Data were fitted using nonlinear regression, as described in Material and Methods, where  $r^2$  was 0.907 for WT and 0.909 for KO.  $N = 6$  WT and 8 KO, age: P40–P50.

et al., 2003). Furthermore, SynCAM 1 KO mice show distinct functional deficits in the rod (scotopic) pathway (Fig. 3B,D). We therefore hypothesized that SynCAM 1 is involved in the organization of rod photoreceptors and their synapses in the OPL. To address this question, we studied the structure and morphology of the retina in adult SynCAM 1 KO mice. To control for potential variations in retinal morphology caused by

light exposure (Balkema and Drager, 1985), and because rod responses were specifically impaired in SynCAM 1 KO mice, all experiments were performed on dark-adapted animals (scotopic conditions).

Gross retinal morphology in adult SynCAM 1 KO mice appeared intact compared with that of their WT littermates, with all layers present and no obvious abnormalities (data not shown). However, upon closer examination,

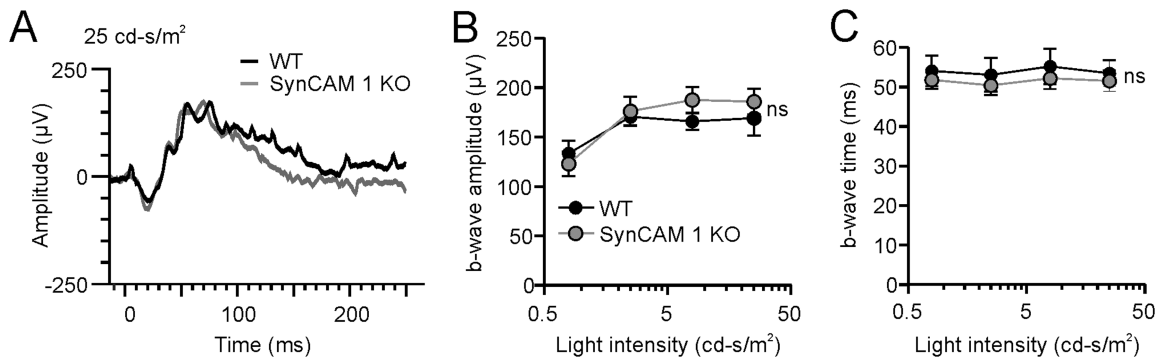


**Figure 4.** Cone pathway is not affected in SynCAM 1 KO mice. **A:** Representative original photopic ERG traces from SynCAM 1 KO and WT mice (5–7 weeks old) at highest light intensity used (25 cd<sup>-s</sup>/m<sup>2</sup>). **B:** Amplitude of photopic b-wave is normal in SynCAM 1 KO mice. **C:** Time-to-peak of photopic b-wave is unaffected in SynCAM 1 KO mice. Differences between groups were analyzed by two-way RM ANOVA: ns, not significant. N = 9 WT and 12 KO, age: P40–P50.

we found that SynCAM 1 KO mice have 12% and 20% thinner outer nuclear layer (ONL) and OPL, respectively, compared with WT mice ( $KO_{OPL} = 9.43 \pm 0.05 \mu\text{m}$ ,  $WT_{OPL} = 10.73 \pm 0.34 \mu\text{m}$ , N = 3,  $P = 0.019$ ;  $KO_{ONL} = 25.25 \pm 1.34 \mu\text{m}$ ,  $WT_{ONL} = 31.42 \pm 0.26 \mu\text{m}$ , N = 3,  $P = 0.01$ ; Student's *t*-test, N = 3/group). The thickness of other layers was comparable in KO and WT mice (data not shown), as was the overall width of the central retina (WT =  $154 \pm 2 \mu\text{m}$ , KO =  $157 \pm 12 \mu\text{m}$ ; N = 3/group). The density of nuclei in the ONL was not significantly different between KO and WT as measured in semi-thick sections of central retina (WT =  $0.15 \pm 0.01$  nuclei/ $\mu\text{m}^3$ ; KO =  $0.14 \pm 0.04$  nuclei/ $\mu\text{m}^3$ ; N = 3/group), making it unlikely that the reduced ONL thickness in SynCAM 1 KO mice was due to a decreased density of photoreceptors.

We next examined general retinal morphology using previously described markers of different retinal cell types (Hoon et al., 2009). Photoreceptor terminals labeled with antibodies against VGlut1 and PSD-95 (Koulen et al., 1998) appeared normal in distribution and intensity in KO mice (Fig. 5A–D). Synaptic ribbons labeled with antibody against Ribeye exhibited their typical horseshoe shape in both WT and KO mice and had an apparently normal distribution and intensity in KO mice (Fig. 5E,F; Regus-Leidig et al., 2010; Schmitz et al., 2000). As expected from the photopic ERG recordings, labeling with PNA showed a normal distribution of cone terminals in the OPL of SynCAM 1 KO mice (Fig. 5G,H; Hoon et al., 2009). The morphology of rod bipolar cells analyzed with anti- $\text{PKC}\alpha$  antibody (Ruether et al., 2010) was indistinguishable between WT and SynCAM 1 KO mice, nor were any differences observed for bipolar cell dendritic tips labeled with antibody against mGluR6 (Fig. 5I–L; Cooper et al., 2012). However, horizontal cells exhibited morphological

defects in SynCAM 1 KO mice (Fig. 5M–P). The horizontal cell marker Calbindin (Hirano et al., 2011) was detected in an ordered series of horizontal cell bodies just above the OPL in WT mice, whereas Neurofilament staining showed their processes extending through the OPL, but never crossing into the ONL (Fig. 5M; Bayley and Morgans, 2007). In contrast, horizontal cell processes in SynCAM 1 KO mice sprouted into the ONL (Fig. 5N). Horizontal cell axons labeled with Neurofilament antibody exhibited ectopic growth, whereas Calbindin staining appeared patchy and disorganized compared with WT (Fig. 5N, arrowheads). Similar to Neurofilament labeling, Calbindin-positive processes also sprouted into the ONL of KO mice (Fig. 5N, arrowheads). We did not detect ectopic ribbons in the SynCAM 1 KO ONL with anti-Ribeye antibodies (Fig. 5P), nor did we detect an altered distribution of general inner nuclear, inner plexiform, and ganglion cell layer (INL, IPL, and GCL, respectively) markers (data not shown). In addition, we did not detect any abnormalities in glial fibrillary acidic protein (GFAP) or vimentin staining in SynCAM 1 KO retinas, indicating absence of retinal degeneration (data not shown). SynCAM 1 KO mice hence exhibit impairments in retinal morphology that appeared limited to the ONL and OPL as well as to horizontal cells.

### Loss of SynCAM 1 impairs morphological development of horizontal cells

Thinning of retinal layers, as well as sprouting of bipolar and horizontal cells, has been commonly observed in aged mouse retina (Matsuoka et al., 2012; Samuel et al., 2011). Adult SynCAM 1 KO mice exhibited sprouting of horizontal cell processes (Fig. 5M–P), so we proceeded to determine if this is due to

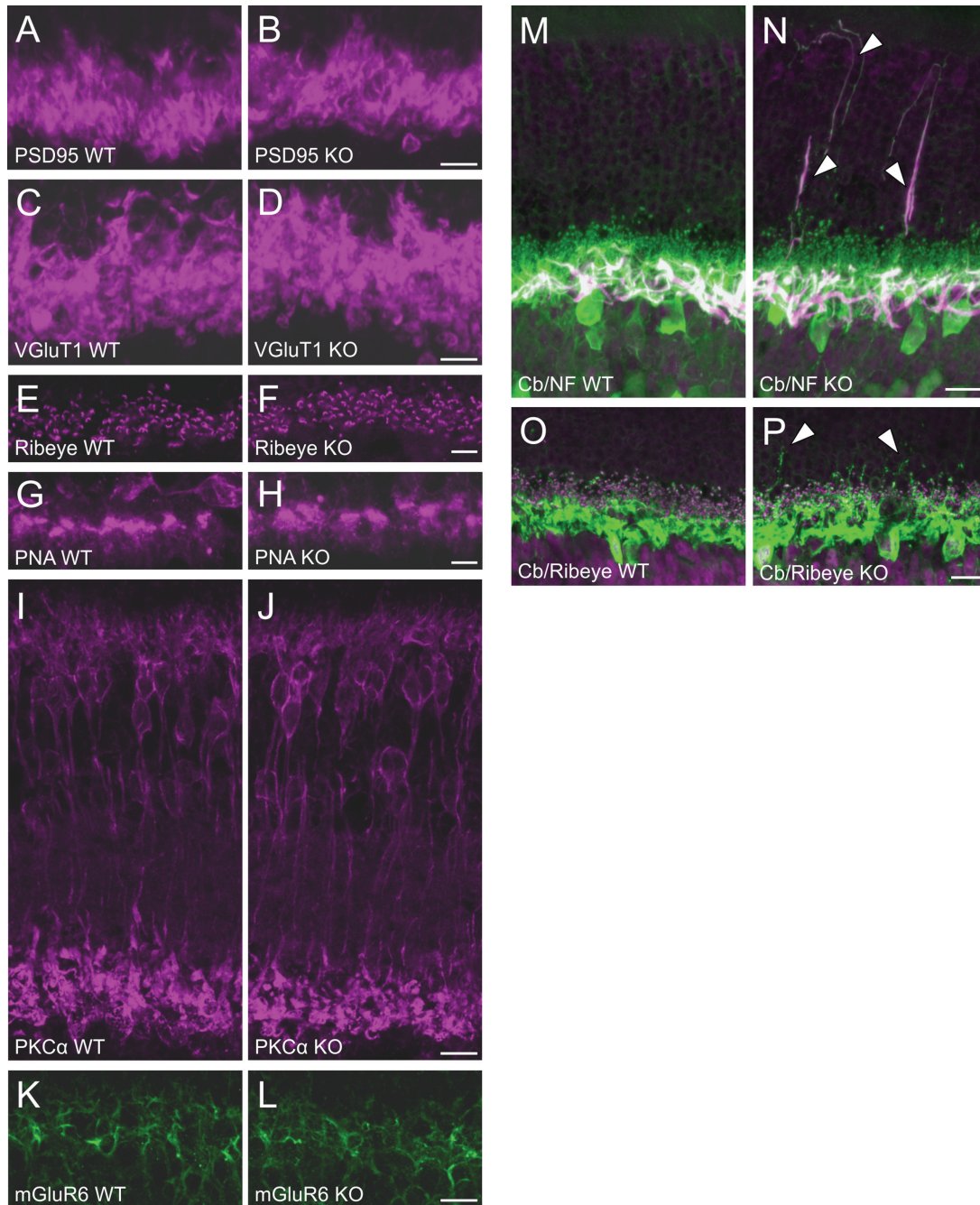


**Figure 5.** SynCAM 1 KO mice display morphological defects of horizontal cell processes in the outer retina. **A–D:** Photoreceptor terminals labeled with PSD-95 (A) and VGLUT1 (C) had a normal appearance in SynCAM 1 KO mice (B,D). **E,F:** Synaptic ribbons labeled with anti-Ribeye also displayed apparently normal distribution at a macroscopic level (but see Fig. 7 and Table 2 for structural aberrations). **G,H:** Cone terminals labeled with PNA also showed normal intensity and distribution in SynCAM 1 KO animals. **I,J:** Rod bipolar cells displayed normal morphology in KO mice shown by immunostaining with antibodies against PKC $\alpha$ . **K,L:** Bipolar cell dendritic tips labeled with mGluR6 also displayed normal morphology. **M,N:** Antibodies against Calbindin (green) and Neurofilament (magenta) demonstrated a regular arrangement of horizontal cell bodies and their processes in WT mice (M). In contrast, KO mice (N) showed sprouting of horizontal cell processes into the ONL (arrowheads). **O,P:** Antibody staining against Calbindin (green) and Ribeye (magenta) of WT (O) and SynCAM 1 KO (P) showed that ectopic cell processes in the KO did not have ribbons apposing them in the ONL. All images are representative maximum-intensity projections of Z-stacks through central retina in  $N = 3$  mice/group (5–7 weeks old). Cb, Calbindin; NF, Neurofilament. Scale bars = 5  $\mu\text{m}$  in A–H; 15  $\mu\text{m}$  in I–L,M,N; 15  $\mu\text{m}$ ; 20  $\mu\text{m}$  in O,P.

premature aging or impairment in the development of horizontal cells. We compared Calbindin immunoreactivity between WT and SynCAM 1 KO retinas at differ-

ent ages (Fig. 6A–H; Matsuoka et al., 2012). At P4, Calbindin-positive cells, as well as the initial network of their lateral processes, could already be seen

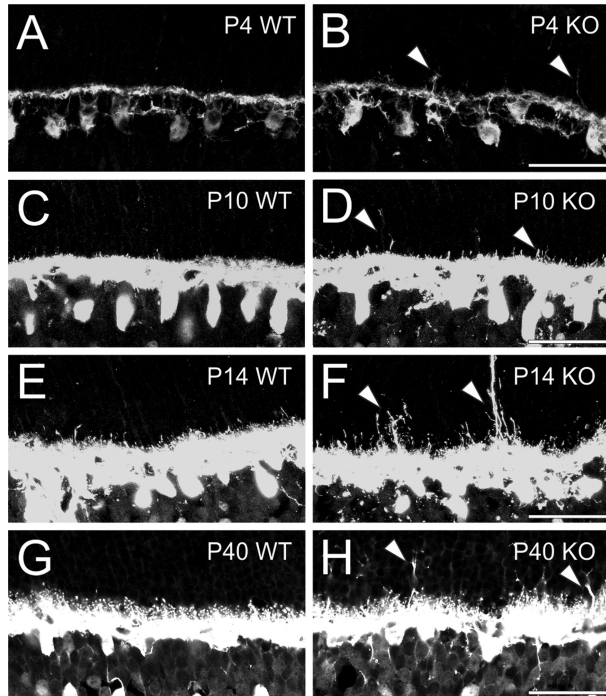


**Figure 6.** Horizontal cell development is impaired in SynCAM 1 KO mice. **A,C,E,G:** Calbindin immunostaining of WT retinas at different ages depicts gradual development of the horizontal cell plexus in the OPL. Horizontal cell bodies are seen arranged just above the OPL, with their processes never crossing into the ONL. **B,D,F,H:** In contrast, horizontal cell processes are seen crossing into ONL at all ages examined in SynCAM 1 KO mice. Ectopic growth is very prominent at P14 and in the adult SynCAM 1 KO retina. Scale bars = 30  $\mu\text{m}$ .

arranged in a single layer in both WT and SynCAM 1 KO mice (Fig. 6A,B; Sharma et al., 2003). The density of the processes increased by P10, when OPL has already formed in both WT and SynCAM 1 KO mice (Fig. 6C,D). However, at both P4 and P10, horizontal cell processes could be seen extending outside of the OPL in SynCAM 1 KO retinas (Fig. 6B,D), unlike in WT retinas (Fig. 6A,C; Sharma et al., 2003). Final stages of triad formation at P14 (Blanks et al., 1974b) revealed a rich plexus of horizontal cell processes in the WT retina (Fig. 6E). It is at this stage when the sprouting in SynCAM 1 KO retina became prominent (Fig. 6F, arrowheads). Calbindin-stained processes could be seen in the P14 KO retina extending throughout the entire ONL, similar to what we observed in adult KO retina (Figs. 5N, 6H). We have not observed alterations in the development and morphology of bipolar cells in SynCAM 1 KO retinas by PKC $\alpha$  staining at any developmental stage we examined (P10, P14, and adult/P40; data not shown). These results indicate that a likely cause for the presence of ectopic horizontal cell neurites in adult SynCAM 1 KO retina is

a defect in horizontal cells development and not premature retinal degeneration.

### Ultrastructure and molecular composition of rod ribbon synapses are altered in SynCAM 1 KO mice

The distribution of synaptic markers in the OPL appeared normal in KO mice at a light microscopic level (Fig. 5A–H). However, SynCAM 1 KO mice display functional defects in the rod visual pathway (Fig. 3A–D). Loss of SynCAM 1 results in functional and ultrastructural abnormalities in classical excitatory synapses as represented by hippocampal synapses in CA1 (Robbins et al., 2010), so we examined the ultrastructure of SynCAM 1 KO photoreceptors and their synapses in the OPL to detect fine structural abnormalities that might account for functional impairments seen in ERGs of SynCAM 1 KO mice.

We measured the ultrastructural parameters of ONL, IS and OS (number of nuclei, internuclear distance, cell body size, length and width of OS and IS, and number and distribution of membranous discs in OS) but were unable to detect any abnormalities in the structure of photoreceptor cell bodies or their IS and OS (data not shown). We then studied ribbon synapses formed among rod photoreceptors, bipolar cells, and horizontal cells. Ribbon synapses are characterized by an electron-dense, plate-like structure called the ribbon, anchored to the membrane of presynaptic photoreceptor terminals (Schmitz, 2009). It is decorated with synaptic vesicles and is involved in tonic vesicle release from photoreceptor terminals (Snellman et al., 2011). When viewed in cross-section, ribbons appear as elongated structures anchored to the photoreceptor plasma membrane and in direct apposition to bipolar cell dendrites in the OPL, with horizontal cell processes settled laterally (Fig. 7A,B, top; tom Dieck and Brandstätter, 2006). All triad elements of ribbon synapses are present in SynCAM 1 KO mice (Fig. 7B, bottom). Synaptic vesicles fill the terminal and are anchored to the ribbon in both WT and KO mice (Fig. 7). We used stereology to quantify a range of parameters of ribbon synapse ultrastructure (Table 2). As expected, we detected very few cone terminals in our sections (Carter-Dawson and LaVail, 1979), and they were excluded from this quantitative analysis. The results revealed significant differences in rod terminal structure between WT and KO mice. Although the density of rod terminals in sections of KO mouse retina was similar to that of WT mice, the number of ribbon-containing rod terminals was significantly lower in SynCAM 1 KO mice (Table 2). In addition, the ribbons were shorter by  $27.6 \pm 5.8\%$  in KO mice. Rod terminal perimeter was also reduced by

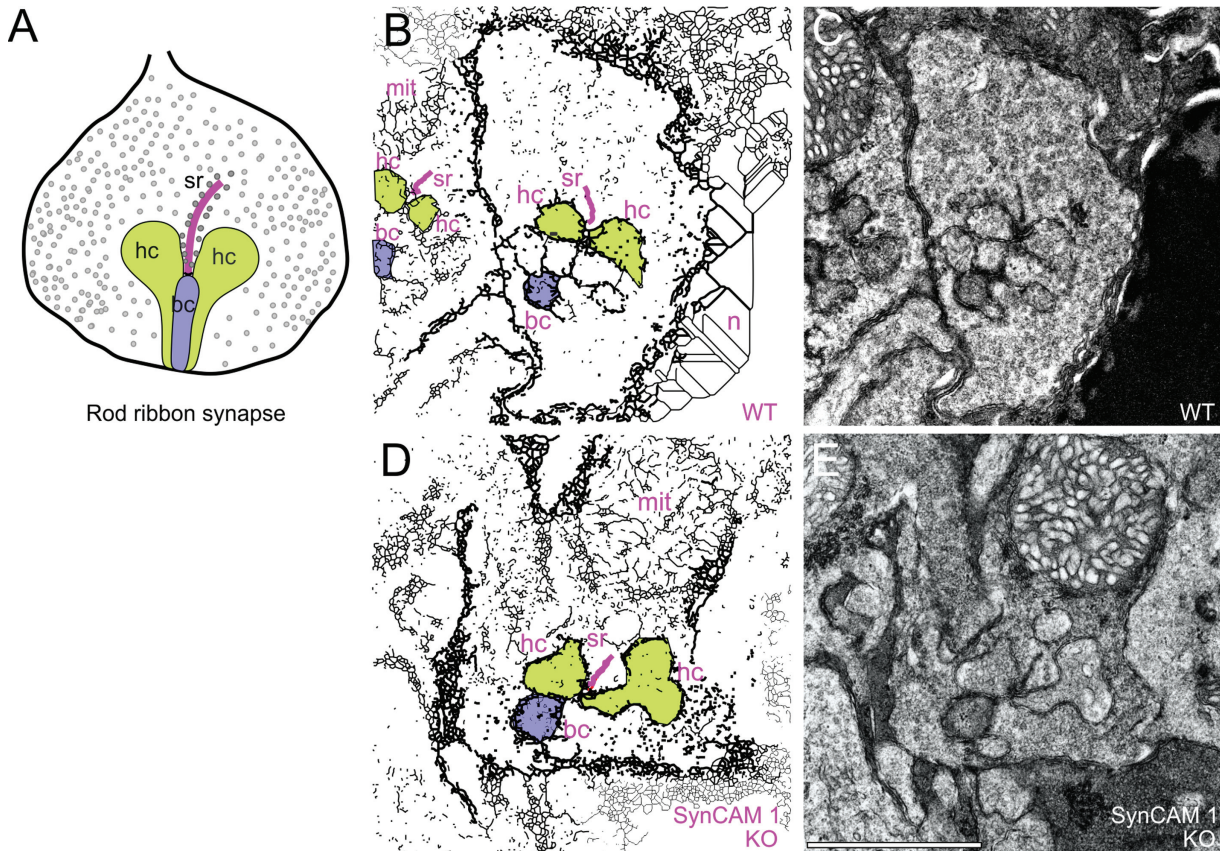


**Figure 7.** SynCAM 1 KO mice have defects in the ultrastructure of ribbon synapses. **A:** Schematic depiction of a rod terminal and its ribbon synapse. A synaptic ribbon (sr, magenta) is shown as an elongated structure opposed bipolar cell dendrites (bc, blue), with horizontal cell processes settled laterally (hc, green). **B:** Top: Trace outline of a representative WT (P40–P45) rod ribbon synapse electron micrograph. Relevant structures are labeled and color-coded for easier identification and comparison with the schematic structure (A). Bottom: Trace outline (D) of a representative SynCAM 1 KO (P40–P45) rod ribbon synapse (E). All elements of the triad are present. For quantification of ultrastructural measurements see Table 2. mit, Mitochondria; n, nucleus; sr, synaptic ribbon; hc, horizontal cell processes; bc, bipolar cell dendrites. Scale bar = 1  $\mu$ m.

$12.2 \pm 1.5\%$  compared with WT mice. Furthermore, the fraction of terminals with triads in KO mice was almost half the value of their WT littermates (KO =  $56 \pm 5.5\%$  of WT). To assess ultrastructural properties of horizontal and bipolar cell processes, we measured their perimeter in rod terminals and found a significant reduction in the size of horizontal ( $18.2 \pm 5.8\%$  compared with WT), but not bipolar, cell processes. Several other parameters were unchanged in KO mice, such as the number of dyads, terminals with multiple ribbons, and nonassociated lateral elements (Table 2). We also found no difference between WT and KO mice in vesicle density (Table 2).

To determine further the extent of changes in ribbons in SynCAM 1 KO mice, we measured their length and density throughout different developmental stages of the retina in high-resolution images obtained via confocal microscopy using an antibody against Ribeye (Fig.

8). Ribeye immunoreactivity in both WT and SynCAM 1 KO mice was in agreement with previously published studies (Regus-Leidig et al., 2009). Ribeye-stained spheres could be detected as early as P4 in both WT and KO mice (Fig. 8A,B), without any differences in their density between the genotypes (Fig. 8J). Horseshoe-shaped ribbons were detectable at P10 in both WT and KO (Fig. 8C,D). The length and the density of horseshoe-shaped ribbons increased at P14 in WT retina (Fig. 8E,F,I,J), but spheres were still detectable (Regus-Leidig et al., 2009). Ribbons of SynCAM 1 KO mice at P14 were of almost identical in length to WT ribbons (Fig. 8I). By P40, all Ribeye-stained objects were horseshoe shaped (Fig. 8G,H). In agreement with the ultrastructural measurements performed in adult retinas, we observed a significant reduction of ribbon length in P40 SynCAM 1 KO mice by  $11 \pm 2.2\%$  compared with WT retina. Moreover, the density of ribbons

**TABLE 2.**  
**Synaptic Parameters Quantified in SynCAM 1 KO Mice<sup>1</sup>**

Parameter	WT	SynCAM 1 KO
Rod terminal number/ $\mu\text{m}^3$	0.26 $\pm$ 0.04	0.27 $\pm$ 0.01
Rod terminal perimeter ( $\mu\text{m}$ )	18.68 $\pm$ 0.71 (60 terminals from N = 3 mice)	16.4 $\pm$ 0.28* (61 terminals from N = 3 mice)
Rod ribbon height (nm)	509 $\pm$ 27 (105 ribbons from N = 3 mice)	369 $\pm$ 29* (68 ribbons from N = 3 mice)
Terminals with ribbon (% of total terminal number)	74 $\pm$ 3.6 of 64 terminals from N = 3 mice	49 $\pm$ 6.4* of 67 terminals from N = 3 mice
Terminals with triads/ $\mu\text{m}^3$	0.055 $\pm$ 0.006	0.024 $\pm$ 0.003*
Terminals with dyads/ $\mu\text{m}^3$	0.02 $\pm$ 0.003	0.02 $\pm$ 0.005
Terminals with multiple ribbons/ $\mu\text{m}^3$	0.005 $\pm$ 0.0002	0.005 $\pm$ 0.003
Terminals with nonassociated ribbons/ $\mu\text{m}^3$	0.007 $\pm$ 0.004	0.017 $\pm$ 0.007
Terminals with nonassociated lateral elements/ $\mu\text{m}^3$	0.006 $\pm$ 0.001	0.008 $\pm$ 0.003
Number of synaptic vesicles/terminal profile area	470 $\pm$ 53	380 $\pm$ 27
Perimeter of invaginating HC processes ( $\mu\text{m}$ )	4.012 $\pm$ 0.08 (65 lateral elements from N = 3 mice)	3.28 $\pm$ 0.23* (44 lateral elements from N = 3 mice)
Perimeter of invaginating BC processes ( $\mu\text{m}$ )	2.18 $\pm$ 0.05 (100 lateral elements from N = 3 mice)	2.36 $\pm$ 0.08 (67 lateral elements from N = 3 mice)

<sup>1</sup>Significant differences between littermate groups as determined with Student's *t*-test (\**P* < 0.05). All values were averaged per animal before performing the statistical tests. N = 3 WT and 3 KO.

in P40 KO retinas was decreased by 26.8  $\pm$  5.8% (Fig. 8I,J).

We additionally performed quantitative Western blotting of retinal homogenates from dark-adapted adult WT and SynCAM 1 KO retina (Fig. 8K,L). Ribeye protein is the major structural component of ribbons (Schmitz et al., 2000; Zenisek et al., 2004). Interestingly, we found that the level of Ribeye protein was reduced by 36  $\pm$  3.8% in SynCAM 1 KO retina consistent with the reduction in ribbon density and size at P40 (Table 2, Fig. 8I–L). Levels of other synaptic proteins (SNAP 25 and SV2) were not significantly changed (data not shown). These results revealed specific alterations in the molecular composition and ultrastructure of ribbon synapses in SynCAM 1 KO mice.

## DISCUSSION

Synaptic adhesion molecules, as well as extracellular matrix and glial cell proteins, have critical roles in the induction of pre- and postsynaptic structures and their assembly into classical synapses (Eroglu and Barres, 2010; Missler et al., 2012). Adhesion molecules also contribute to the formation of classical synapses in the inner retina (Fuerst and Burgess, 2009), but their roles in the development of outer retinal layers remain incompletely understood. Analyzing the retina, we report here the selective enrichment of SynCAM 1 in the outer retinal layers. The loss of SynCAM 1 in turn had significant effects on the structure and function of rod photoreceptors. Our study also points to a novel role for synaptic adhesion beyond classical synapses by

providing evidence that SynCAM 1 functions in the structural modulation of photoreceptor ribbon synapses in the retina.

## Distribution and subcellular localization of SynCAM 1 in the retina

Retinal expression of SynCAM 1 has been reported in different species, including mice (Fujita et al., 2005; Pietri et al., 2008; Wahlin et al., 2008). However, a detailed study on the expression and function of retinal SynCAM 1 has been lacking. This study shows for the first time that SynCAM 1 is expressed throughout the developing and adult mouse retina and that SynCAM 1 is particularly enriched on cell bodies and terminals of mature rod photoreceptors. This is also the first study to demonstrate in ultrastructural detail the specific localization of endogenous SynCAM 1 in the CNS. Antibodies used in a previous study (Biederer et al., 2002) recognize SynCAMs 1, 2, and 3 equally well (Fogel et al., 2007), and the precise localization of SynCAM 1 in the CNS remained to be determined (Fogel et al., 2011). Our immuno-EM study of photoreceptors detected endogenous SynCAM 1 at their synaptic terminal membranes (Fig. 2). These findings significantly expand previous studies of SynCAM 1 localization at classical synapses by light microscopic analysis of hippocampus (Fogel et al., 2011) and the presynaptic localization of exogenously expressed SynCAM 1 detected by EM in cultured cortical neurons (Shu et al., 2011). As our light microscopy had already suggested (Fig. 2), SynCAM 1 was not concentrated at synaptic

sites in the OPL but was evenly distributed on the terminal membrane, indicating roles in cell surface interactions throughout this synaptic region. In agreement with general roles in the organization of photoreceptor synaptic membranes, we additionally detected SynCAM 1

at the interface of photoreceptor terminals and horizontal cell processes. SynCAM 1 was also found in other retinal layers (Fig. 1), but its relative abundance in the photoreceptor layer agrees with a role in the structural and functional integrity of photoreceptors and their synapses.

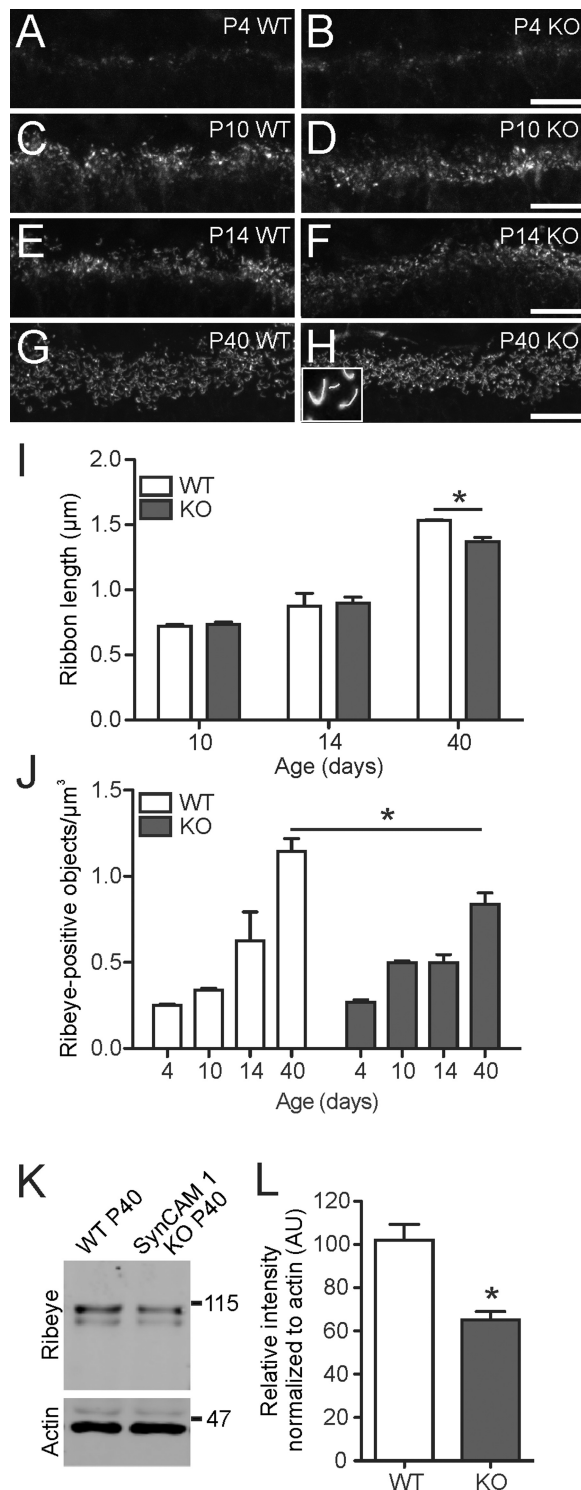


Figure 8.

### Modulation of retinal function by SynCAM 1

Our ERG recordings demonstrated that visual signal transmission in the scotopic (rod) pathway is impaired in SynCAM 1 KO mice. Normal double-flash ERG responses, the apparent lack of retinal degeneration indicated by normal appearance of glial markers (data not shown), as well as the overall normal ultrastructure of the ONL and OS (data not shown), suggest that these functional differences do not stem from altered photoreceptor number or the ultrastructure of their cell bodies and OSs. The importance of gap junction adhesion proteins in synaptic transmission at the OPL is well known (Bloomfield and Volgyi, 2009; Kamermans et al., 2001; Kranz et al., 2012). Our study for the first time implicates a classical synaptic adhesion molecule (Missler et al., 2012) in the rod visual pathway.

The increased scotopic a-wave that we measured in SynCAM 1 KO mice is extremely rare in animal models of retinal dysfunction (Brockerhoff et al., 1997; Kameya et al., 1997; Kranz et al., 2012) and could be a cause of delay in b-wave time-to-peak in SynCAM 1 KO mice. What might cause this enhanced amplitude of rod responses to light? This effect of SynCAM 1 loss might be due to abnormal phototransduction in the OSs (Knop et al., 2008; Liu et al., 2005; Seeliger et al., 2011). This is usually assessed with double-flash ERG,

**Figure 8.** Ribbons are sparse and shortened and Ribeye levels are reduced in adult SynCAM 1 KO mice. **A–H:** Representative images of Ribeye staining in WT and SynCAM 1 KO mice at different ages. **Inset** shows an outline of ribbon length measurement. Statistical analysis performed with two-way ANOVA revealed no interaction between the age and the genotype for both length and density of ribbons as well as no effects of genotype on either ribbon length or density (length:  $F_{1,10} = 0.0949$ ,  $P = 0.353$ ; density:  $F_{1,13} = 1.169$ ,  $P = 0.299$ ). **I:** Ribbon length in KO animals was significantly reduced only in adult (P40) animals as shown by post hoc Holm-Sidak test ( $*P = 0.016$ ; WT =  $1.53 \pm 0.007 \mu\text{m}$ , KO =  $1.37 \pm 0.03 \mu\text{m}$ ). **J:** Post hoc Holm-Sidak test revealed that ribbon density was reduced only in adult KO animals ( $*P = 0.02$ ; WT =  $1.14 \pm 0.08/\mu\text{m}^3$ , KO =  $0.84 \pm 0.07/\mu\text{m}^3$ ;  $N = 3/\text{group}$ ).  $N = 3$  WT and 2 KO for P4–P14,  $N = 3$  WT and 3 KO for P40. **K,L:** SynCAM 1 KO mice show a significant decrease ( $*P = 0.012$ ) in the abundance of Ribeye as determined by quantitative immunoblotting of P40 dark-adapted retinas (KO =  $64 \pm 3.8\%$  of WT;  $N = 3/\text{group}$ , Student's  $t$ -test). Scale bars =  $20 \mu\text{m}$ .

which monitors recovery of photoreceptor responses (Lyubarsky and Pugh, 1996). However, recovery was not impaired in SynCAM 1 KO mice. We therefore consider it unlikely that the increased a-wave in SynCAM 1 KO mice stems from a dysfunction of the rod OSs. Alternatively, the functional block of channels that localize near the photoreceptor terminal membrane can affect the a-wave properties (Chang et al., 2006; Kranz et al., 2012; Mansergh et al., 2005). Adhesion molecules organize and cluster different classes of channels on the neuronal membranes (Gu and Gu, 2011; Leterrier et al., 2011; Missler et al., 2003). Hence, a cause of defective a-wave seen in SynCAM 1 KO mice may be impaired clustering of ion channels at the photoreceptor terminal membranes. Because SynCAM 1 organizes synapses in hippocampal neurons (Cheadle and Biederer, 2012; Fogel et al., 2011) and is present at rod terminal membranes in the OPL, this possibility can now be tested.

Recent studies have also highlighted a role of negative feedback from horizontal cells to photoreceptors (Liu et al., 2013). Abnormal development of horizontal cells in SynCAM 1 KO mice, as well as a reduction in the surface area of their processes within ribbon synapses in adult mice, may cause an impairment in negative feedback to rods and hence contribute to the defect in rod response upon light stimulation. The localization of SynCAM 1 near the horizontal cell processes supports this notion. A recent study has suggested such impaired feedback from horizontal cells to rod photoreceptors as a cause of increased a-wave amplitude in mice lacking Pannexin1, a membrane protein related to the gap-junction-forming connexins (Kranz et al., 2012). Scotopic a-wave also has postreceptor contributions, mainly from the OFF pathway (Dang et al., 2011; Robson and Frishman, 1998). Additionally, Müller cells can contribute to photoreceptor responses (Witkovsky et al., 1975). However, we did not detect SynCAM 1 on Müller glia, and we did not observe any abnormalities in their morphology or the morphology of bipolar cells (data not shown), which makes their involvement in SynCAM 1 functions unlikely. Because of the mixed nature of the ERG response (Robson and Frishman, 1998), the precise origin of impairments in scotopic ERG of SynCAM 1 KO mice remains to be defined.

### Altered structural and molecular organization of photoreceptor ribbon synapses in the absence of SynCAM 1

The temporal and spatial expression profile of SynCAM 1 closely follows the structural and functional development of outer retinal layers and photoreceptor

synapses. A key finding in support of a role for SynCAM 1 in the formation of these synapses is the decrease in density of terminals with ribbons in SynCAM 1 KO mice by  $28.4 \pm 9.3\%$ . Perhaps even more importantly, KO mice have a significant  $56 \pm 5.5\%$  reduction in the number of synaptic triads formed among rod terminals, bipolar cell dendrites, and horizontal cell processes. No other structural abnormalities were observed, such as free-floating or club-shaped ribbons seen in other mouse models with retinal defects (Dick et al., 2003; Reim et al., 2009). The number of other structures in retinal sections (dyads between rod spherules and horizontal cells, for example) was surprisingly unaffected in KO mice, contrasting with other mutants in which a reduction in triad density is closely correlated with an increase in dyad density (Blanks et al., 1974a; Bramblett et al., 2004; Sato et al., 2008). The significant reduction in Ribeye protein expression in adult SynCAM 1 KO retina provides biochemical support for these structural results in rod photoreceptor terminals. Ribeye is the core structural component of ribbons (Zanazzi and Matthews, 2009), both in the OPL and in the IPL (Johnson et al., 2003). Although a decrease in its expression in IPL synapses of SynCAM 1 KO mice may contribute to its observed overall reduction in their retina, Ribeye is enriched in the OPL compared with the IPL (Schmitz et al., 2000). The Ribeye reduction in SynCAM 1 KO mice therefore likely reflects changes in the OPL. The reduced Ribeye level in adult KO retina further agrees with the reduction of ribbon density and length observed here.

SynCAM 1 in the hippocampus contributes to both early stages of synapse induction and their later maintenance (Robbins et al., 2010). The developmental expression profile of SynCAM 1 in the retina would agree with synaptogenic functions, because the formation of synapses in the OPL starts at about P5 (Sharma et al., 2003). Results of our study demonstrated that ribbons in SynCAM 1 KO mice develop normally until P14 and that their number and length are reduced only in adult animals. Final stages of triad formation occur at P14 (Blanks et al., 1974a), and SynCAM 1 expression in the retina continues to increase after P14. Together, these findings point to roles of SynCAM 1 in the final steps of the assembly of rod ribbon synapses and their maintenance.

An unexpected finding of this study related to the development of outer retina is that SynCAM 1 may guide proper development and targeting of horizontal cell processes in the OPL (Sharma et al., 2003). Ectopic horizontal cell processes can be seen as early as P4 in SynCAM 1 KO mice, and their development appeared abnormal at all later stages examined. No abnormalities were

detected in the morphology of bipolar cells in SynCAM 1 KO mice (data not shown), which differs for the coupled horizontal and bipolar cell aberrations, e.g., in mice carrying mutations in ribbon synapse proteins (Dick et al., 2003; Haeseleer et al., 2004; Strettoi et al., 2002). The selective effect of SynCAM 1 loss on horizontal cell differentiation is reminiscent of mice deficient in Plexin/Semaphorin signaling as well as mice lacking adhesive interactions by the protein NGL-2 (Matsuoka et al., 2012; Soto et al., 2013). SynCAM 1-mediated cell surface interactions may therefore contribute to the proper targeting of horizontal cell neurites during development, perhaps reminiscent of the roles of this protein in shaping axonal growth cones (Stagi et al., 2010).

### SynCAM 1 in classical vs. ribbon synapses: evidence for general contributions to synapse organization and function

Roles of SynCAM 1 at classical synapses have been well described (Fogel et al., 2007; Robbins et al., 2010). The reduced triad numbers and shortened ribbons in the KO retina are consistent with the decreased synapse density and shortened active zones in the hippocampus (Robbins et al., 2010). Unlike neuroligins (Hoon et al., 2009, 2011) or other immunoglobulin-family proteins, such as DSCAMs (Fuerst et al., 2009), that contribute to the development and function of the IPL, SynCAM 1 in the retina appears predominantly to provide for the structural and functional integrity of photoreceptor synapses in the OPL. To the best of our knowledge, SynCAM 1 is the first synaptic adhesion molecule with complementary roles at different types of synapses, including ribbon synapses.

The results that we obtained from the outer retina extend the well-defined effects of adhesion molecules on cell and synapse specification of the inner retina (Yamagata and Sanes, 2012). Furthermore, these findings indicate a general role for SynCAM 1-mediated adhesion in the organization of excitatory synapses and neuronal circuits, such as reported here. Our results warrant studies of visual signal processing in KO mice, especially considering that they show sufficient vision in gross behavioral vision assays (Robbins et al., 2010).

### ACKNOWLEDGMENTS

We thank the members of the Biederer and Crair laboratories for support and discussions. We are grateful to S. Mentone and M. Graham for processing of EM samples, Y. Lei for technical assistance, and Dr. O.S. Dhande for technical and intellectual input. We also thank Drs. Bo Chen, Sreeganga Chandra, In-Jung Kim, Jun Lin, and David Zenisek for valuable reagents and indispensable advice.

### CONFLICT OF INTEREST STATEMENT

The authors declare no conflict of interest.

### ROLE OF AUTHORS

All authors had full access to all the data in the study and take responsibility for the integrity of the data and the accuracy of the data analysis. Study concept and design: AR, MCC, TB. Acquisition of data: AR, XL. Analysis and interpretation of data: AR, XL, MCC, TB. Drafting of the manuscript: AR, TB. Critical revision of the manuscript for important intellectual content: XL, MCC. Statistical analysis: AR. Obtained funding: TB, AR, MCC. Technical and material support: XL, MCC. Study supervision: TB.

### LITERATURE CITED

- Abd-El-Barr MM, Pennesi ME, Saszik SM, Barrow AJ, Lem J, Bramblett DE, Paul DL, Frishman LJ, Wu SM. 2009. Genetic dissection of rod and cone pathways in the dark-adapted mouse retina. *J Neurophysiol* 102:1945–1955.
- Balkema GW, Drager UC. 1985. Light-dependent antibody labelling of photoreceptors. *Nature* 316:630–633.
- Bayley PR, Morgans CW. 2007. Rod bipolar cells and horizontal cells form displaced synaptic contacts with rods in the outer nuclear layer of the nob2 retina. *J Comp Neurol* 500:286–298.
- Biederer T, Sara Y, Mozhayeva M, Atasoy D, Liu X, Kavalali ET, Südhof TC. 2002. SynCAM, a synaptic adhesion molecule that drives synapse assembly. *Science* 297:1525–1531.
- Blanks JC, Adinolfi AM, Lolley RN. 1974a. Photoreceptor degeneration and synaptogenesis in retinal-degenerative (rd) mice. *J Comp Neurol* 156:95–106.
- Blanks JC, Adinolfi AM, Lolley RN. 1974b. Synaptogenesis in the photoreceptor terminal of the mouse retina. *J Comp Neurol* 156:81–93.
- Bloomfield SA, Volgyi B. 2009. The diverse functional roles and regulation of neuronal gap junctions in the retina. *Nat Rev Neurosci* 10:495–506.
- Bramblett DE, Pennesi ME, Wu SM, Tsai MJ. 2004. The transcription factor Bhlhb4 is required for rod bipolar cell maturation. *Neuron* 43:779–793.
- Brockerhoff SE, Hurley JB, Niemi GA, Dowling JE. 1997. A new form of inherited red-blindness identified in zebrafish. *J Neurosci* 17:4236–4242.
- Brown KT, Watanabe K. 1962a. Isolation and identification of a receptor potential from the pure cone fovea of the monkey retina. *Nature* 193:958–960.
- Brown KT, Watanabe K. 1962b. Rod receptor potential from the retina of the night monkey. *Nature* 196:547–550.
- Brown KT, Watanabe K, Murakami M. 1965. The early and late receptor potentials of monkey cones and rods. *Cold Spring Harbor Symp Quant Biol* 30:457–482.
- Carter-Dawson LD, LaVail MM. 1979. Rods and cones in the mouse retina. I. Structural analysis using light and electron microscopy. *J Comp Neurol* 188:245–262.
- Chang B, Heckenlively JR, Bayley PR, Brecha NC, Davissou MT, Hawes NL, Hirano AA, Hurd RE, Ikeda A, Johnson BA, McCall MA, Morgans CW, Nusinowitz S, Peachey NS, Rice DS, Vessey KA, Gregg RG. 2006. The nob2 mouse, a null mutation in *Cacna1f*: anatomical and functional abnormalities in the outer retina and their consequences on ganglion cell visual responses. *Vis Neurosci* 23:11–24.

- Cheadle L, Biederer T. 2012. The novel synaptogenic protein Farp1 links postsynaptic cytoskeletal dynamics and transsynaptic organization. *J Cell Biol* 199:985–1001.
- Cooper B, Hemmerlein M, Ammermüller J, Imig C, Reim K, Lipstein N, Kalla S, Kawabe H, Brose N, Brandstätter JH, Varoqueaux F. 2012. Munc13-independent vesicle priming at mouse photoreceptor ribbon synapses. *J Neurosci* 32:8040–8052.
- Dang TM, Tsai TI, Vingrys AJ, Bui BV. 2011. Post-receptor contributions to the rat scotopic electroretinogram a-wave. *Doc Ophthalmol Adv Ophthalmol* 122:149–156.
- Dick O, tom Dieck S, Altrock WD, Ammermüller J, Weiler R, Garner CC, Gundelfinger ED, Brandstätter JH. 2003. The presynaptic active zone protein bassoon is essential for photoreceptor ribbon synapse formation in the retina. *Neuron* 37:775–786.
- Duncan JL, Yang H, Doan T, Silverstein RS, Murphy GJ, Nune G, Liu X, Copenhagen D, Tempel BL, Rieke F, Krizaj D. 2006. Scotopic visual signaling in the mouse retina is modulated by high-affinity plasma membrane calcium extrusion. *J Neurosci* 26:7201–7211.
- Ekesten B, Gouras P, Moschos M. 1998. Cone properties of the light-adapted murine ERG. *Doc Ophthalmol Adv Ophthalmol* 97:23–31.
- Eroglu C, Barres BA. 2010. Regulation of synaptic connectivity by glia. *Nature* 468:223–231.
- Fisher LJ. 1979. Development of synaptic arrays in the inner plexiform layer of neonatal mouse retina. *J Comp Neurol* 187:359–372.
- Fogel AI, Akins MR, Krupp AJ, Stagi M, Stein V, Biederer T. 2007. SynCAMs organize synapses through heterophilic adhesion. *J Neurosci* 27:12516–12530.
- Fogel AI, Stagi M, Perez de Arce K, Biederer T. 2011. Lateral assembly of the immunoglobulin protein SynCAM 1 controls its adhesive function and instructs synapse formation. *EMBO J* 30:4728–4738.
- Fuerst PG, Burgess RW. 2009. Adhesion molecules in establishing retinal circuitry. *Curr Opin Neurobiol* 19:389–394.
- Fuerst PG, Bruce F, Tian M, Wei W, Elstrott J, Feller MB, Erskine L, Singer JH, Burgess RW. 2009. DSCAM and DSCAML1 function in self-avoidance in multiple cell types in the developing mouse retina. *Neuron* 64:484–497.
- Fujita E, Urase K, Soyama A, Kouroku Y, Momoi T. 2005. Distribution of RA175/TSLC1/SynCAM, a member of the immunoglobulin superfamily, in the developing nervous system. *Brain Res Dev Brain Res* 154:199–209.
- Fujita E, Kouroku Y, Ozeki S, Tanabe Y, Toyama Y, Maekawa M, Kojima N, Senoo H, Toshimori K, Momoi T. 2006. Oligo-astheno-teratozoospermia in mice lacking RA175/TSLC1/SynCAM/IGSF4A, a cell adhesion molecule in the immunoglobulin superfamily. *Mol Cell Biol* 26:718–726.
- Fujita E, Tanabe Y, Hirose T, Aurrand-Lions M, Kasahara T, Imhof BA, Ohno S, Momoi T. 2007. Loss of partitioning-defective-3/isotype-specific interacting protein (par-3/ASIP) in the elongating spermatid of RA175 (IGSF4A/SynCAM)-deficient mice. *Am J Pathol* 171:1800–1810.
- Gu C, Gu Y. 2011. Clustering and activity tuning of Kv1 channels in myelinated hippocampal axons. *J Biol Chem* 286:25835–25847.
- Haeseleer F, Imanishi Y, Maeda T, Possin DE, Maeda A, Lee A, Rieke F, Palczewski K. 2004. Essential role of Ca<sup>2+</sup>-binding protein 4, a Cav1.4 channel regulator, in photoreceptor synaptic function. *Nat Neurosci* 7:1079–1087.
- Haverkamp S, Wässle H. 2000. Immunocytochemical analysis of the mouse retina. *J Comp Neurol* 424:1–23.
- Heidelberger R, Thoreson WB, Witkovsky P. 2005. Synaptic transmission at retinal ribbon synapses. *Prog Ret Eye Res* 24:682–720.
- Hirano AA, Brandstätter JH, Morgans CW, Brecha NC. 2011. SNAP25 expression in mammalian retinal horizontal cells. *J Comp Neurol* 519:972–988.
- Hoon M, Bauer G, Fritschy JM, Moser T, Falkenburger BH, Varoqueaux F. 2009. Neuroigin 2 controls the maturation of GABAergic synapses and information processing in the retina. *J Neurosci* 29:8039–8050.
- Hoon M, Soykan T, Falkenburger B, Hammer M, Patrizi A, Schmidt KF, Sassoe-Pognetto M, Lowel S, Moser T, Taschenberger H, Brose N, Varoqueaux F. 2011. Neuroigin-4 is localized to glycinergic postsynapses and regulates inhibition in the retina. *Proc Natl Acad Sci U S A* 108:3053–3058.
- Howes KA, Pennesi ME, Sokal I, Church-Kopish J, Schmidt B, Margolis D, Frederick JM, Rieke F, Palczewski K, Wu SM, Detwiler PB, Baehr W. 2002. GCAP1 rescues rod photoreceptor response in GCAP1/GCAP2 knockout mice. *EMBO J* 21:1545–1554.
- Jinno S, Aika Y, Fukuda T, Kosaka T. 1998. Quantitative analysis of GABAergic neurons in the mouse hippocampus, with optical disector using confocal laser scanning microscope. *Brain Res* 814:55–70.
- Johnson J, Tian N, Caywood MS, Reimer RJ, Edwards RH, Copenhagen DR. 2003. Vesicular neurotransmitter transporter expression in developing postnatal rodent retina: GABA and glycine precede glutamate. *J Neurosci* 23:518–529.
- Kamermans M, Fahrenfort I, Schultz K, Janssen-Bienhold U, Sjoerdsma T, Weiler R. 2001. Hemichannel-mediated inhibition in the outer retina. *Science* 292:1178–1180.
- Kameya S, Araki E, Katsuki M, Mizota A, Adachi E, Nakahara K, Nonaka I, Sakuragi S, Takeda S, Nabeshima Y. 1997. Dp260 disrupted mice revealed prolonged implicit time of the b-wave in ERG and loss of accumulation of beta-dystroglycan in the outer plexiform layer of the retina. *Hum Mol Genet* 6:2195–2203.
- Kim TS, Maeda A, Maeda T, Heinlein C, Kedishvili N, Palczewski K, Nelson PS. 2005. Delayed dark adaptation in 11-cis-retinol dehydrogenase-deficient mice: a role of RDH11 in visual processes in vivo. *J Biol Chem* 280:8694–8704.
- Knop GC, Seeliger MW, Thiel F, Mataruga A, Kaupp UB, Friedburg C, Tanimoto N, Muller F. 2008. Light responses in the mouse retina are prolonged upon targeted deletion of the HCN1 channel gene. *Eur J Neurosci* 28:2221–2230.
- Koulen P, Fletcher EL, Craven SE, Brecht DS, Wässle H. 1998. Immunocytochemical localization of the postsynaptic density protein PSD-95 in the mammalian retina. *J Neurosci* 18:10136–10149.
- Kranz K, Dorgau B, Pottke M, Herrling R, Schultz K, Bolte P, Monyer H, Penuela S, Laird DW, Dedek K, Weiler R, Janssen-Bienhold U. 2012. Expression of Pannexin1 in the outer plexiform layer of the mouse retina and physiological impact of its knock-out. *J Comp Neurol* (in press).
- Kueng-Hitz N, Rol P, Niemyer G. 1999. The electroretinogram (ERG) of the mouse: normal values, optimal stimulation and recording. *Klin Monatsblätter Augenheilkunde* 214:288–290.
- Lefebvre JL, Zhang Y, Meister M, Wang X, Sanes JR. 2008. Gamma-protocadherins regulate neuronal survival but are dispensable for circuit formation in retina. *Development* 135:4141–4151.

- Leterrier C, Brachet A, Dargent B, Vacher H. 2011. Determinants of voltage-gated sodium channel clustering in neurons. *Semin Cell Dev Biol* 22:171–177.
- Li J, Cline HT. 2010. Visual deprivation increases accumulation of dense core vesicles in developing optic tectal synapses in *Xenopus laevis*. *J Comp Neurol* 518:2365–2381.
- Liu J, Timmers AM, Lewin AS, Hauswirth WW. 2005. Ribozyme knockdown of the gamma-subunit of rod cGMP phosphodiesterase alters the ERG and retinal morphology in wild-type mice. *Invest Ophthalmol Vis Sci* 46:3836–3844.
- Liu X, Hirano AA, Sun X, Brecha NC, Barnes S. 2013. Calcium channels in rat horizontal cells regulate feedback inhibition of photoreceptors through an unconventional GABA- and pH-sensitive mechanism. *J Physiol* (in press).
- Lyubarsky AL, Pugh EN Jr. 1996. Recovery phase of the murine rod photoresponse reconstructed from electroretinographic recordings. *J Neurosci* 16:563–571.
- Mansergh F, Orton NC, Vessey JP, Lalonde MR, Stell WK, Tremblay F, Barnes S, Rancourt DE, Bech-Hansen NT. 2005. Mutation of the calcium channel gene *Cacna1f* disrupts calcium signaling, synaptic transmission and cellular organization in mouse retina. *Hum Mol Genet* 14:3035–3046.
- Matsuoka RL, Jiang Z, Samuels IS, Nguyen-Ba-Charvet KT, Sun LO, Peachey NS, Chedotal A, Yau KW, Kolodkin AL. 2012. Guidance-cue control of horizontal cell morphology, lamination, and synapse formation in the mammalian outer retina. *J Neurosci* 32:6859–6868.
- Missler M, Zhang W, Rohlmann A, Kattenstroth G, Hammer RE, Gottmann K, Südhof TC. 2003. Alpha-neurexins couple  $Ca^{2+}$  channels to synaptic vesicle exocytosis. *Nature* 423:939–948.
- Missler M, Südhof TC, Biederer T. 2012. Synaptic cell adhesion. *Cold Spring Harbor Perspect Biol* (in press).
- Peachey NS, Ball SL. 2003. Electrophysiological analysis of visual function in mutant mice. *Doc Ophthalmol Adv Ophthalmol* 107:13–36.
- Pietri T, Easley-Neal C, Wilson C, Washbourne P. 2008. Six *cadm/SynCAM* genes are expressed in the nervous system of developing zebrafish. *Dev Dyn* 237:233–246.
- Pinto LH, Invergo B, Shimomura K, Takahashi JS, Troy JB. 2007. Interpretation of the mouse electroretinogram. *Doc Ophthalmol Adv Ophthalmol* 115:127–136.
- Regus-Leidig H, Tom Dieck S, Specht D, Meyer L, Brandstätter JH. 2009. Early steps in the assembly of photoreceptor ribbon synapses in the mouse retina: the involvement of precursor spheres. *J Comp Neurol* 512:814–824.
- Regus-Leidig H, tom Dieck S, Brandstätter JH. 2010. Absence of functional active zone protein Bassoon affects assembly and transport of ribbon precursors during early steps of photoreceptor synaptogenesis. *Eur J Cell Biol* 89:468–475.
- Reim K, Regus-Leidig H, Ammermüller J, El-Kordi A, Radyushkin K, Ehrenreich H, Brandstätter JH, Brose N. 2009. Aberrant function and structure of retinal ribbon synapses in the absence of complexin 3 and complexin 4. *J Cell Sci* 122:1352–1361.
- Robbins EM, Krupp AJ, Perez de Arce K, Ghosh AK, Fogel AI, Boucard A, Südhof TC, Stein V, Biederer T. 2010. SynCAM 1 adhesion dynamically regulates synapse number and impacts plasticity and learning. *Neuron* 68:894–906.
- Robson JG, Frishman LJ. 1998. Dissecting the dark-adapted electroretinogram. *Doc Ophthalmol Adv Ophthalmol* 95:187–215.
- Ruether K, Feigenspan A, Pirngruber J, Leitges M, Baehr W, Strauss O. 2010. PKC $\alpha$  is essential for the proper activation and termination of rod bipolar cell response. *Invest Ophthalmol Vis Sci* 51:6051–6058.
- Samuel MA, Zhang Y, Meister M, Sanes JR. 2011. Age-related alterations in neurons of the mouse retina. *J Neurosci* 31:16033–16044.
- Sato S, Omori Y, Katoh K, Kondo M, Kanagawa M, Miyata K, Funabiki K, Koyasu T, Kajimura N, Miyoshi T, Sawai H, Kobayashi K, Tani A, Toda T, Usukura J, Tano Y, Fujikado T, Furukawa T. 2008. Pikachurin, a dystroglycan ligand, is essential for photoreceptor ribbon synapse formation. *Nat Neurosci* 11:923–931.
- Schmitz F. 2009. The making of synaptic ribbons: how they are built and what they do. *Neuroscientist* 15:611–624.
- Schmitz F, Königstorfer A, Südhof TC. 2000. RIBEYE, a component of synaptic ribbons: a protein's journey through evolution provides insight into synaptic ribbon function. *Neuron* 28:857–872.
- Seeliger MW, Brombas A, Weiler R, Humphries P, Knop G, Tanimoto N, Müller F. 2011. Modulation of rod photoreceptor output by HCN1 channels is essential for regular mesopic cone vision. *Nat Commun* 2:532.
- Shapiro L, Love J, Colman DR. 2007. Adhesion molecules in the nervous system: structural insights into function and diversity. *Annu Rev Neurosci* 30:451–474.
- Sharma RK, O'Leary TE, Fields CM, Johnson DA. 2003. Development of the outer retina in the mouse. *Brain Res Dev Brain Res* 145:93–105.
- Sherry DM, Wang MM, Bates J, Frishman LJ. 2003. Expression of vesicular glutamate transporter 1 in the mouse retina reveals temporal ordering in development of rod vs. cone and ON vs. OFF circuits. *J Comp Neurol* 465:480–498.
- Shu X, Lev-Ram V, Deerinck TJ, Qi Y, Ramko EB, Davidson MW, Jin Y, Ellisman MH, Tsien RY. 2011. A genetically encoded tag for correlated light and electron microscopy of intact cells, tissues, and organisms. *PLoS Biol* 9:e1001041.
- Snellman J, Mehta B, Babai N, Bartoletti TM, Akmentin W, Francis A, Matthews G, Thoreson W, Zenisek D. 2011. Acute destruction of the synaptic ribbon reveals a role for the ribbon in vesicle priming. *Nat Neurosci* 14:1135–1141.
- Song X, Vishnivetskiy SA, Seo J, Chen J, Gurevich EV, Gurevich VV. 2011. Arrestin-1 expression level in rods: balancing functional performance and photoreceptor health. *Neuroscience* 174:37–49.
- Soto F, Watkins KL, Johnson RE, Schottler F, Kerschensteiner D. 2013. NGL-2 regulates pathway-specific neurite growth and lamination, synapse formation, and signal transmission in the retina. *J Neurosci* 33:11949–11959.
- Stagi M, Fogel AI, Biederer T. 2010. SynCAM 1 participates in axo-dendritic contact assembly and shapes neuronal growth cones. *Proc Natl Acad Sci U S A* 107:7568–7573.
- Sterio DC. 1984. The unbiased estimation of number and sizes of arbitrary particles using the disector. *J Microsc* 134:127–136.
- Sterling P, Matthews G. 2005. Structure and function of ribbon synapses. *Trends Neurosci* 28:20–29.
- Strettoi E, Porciatti V, Falsini B, Pignatelli V, Rossi C. 2002. Morphological and functional abnormalities in the inner retina of the rd/rd mouse. *J Neurosci* 22:5492–5504.
- Thomas LA, Akins MR, Biederer T. 2008. Expression and adhesion profiles of SynCAM molecules indicate distinct neuronal functions. *J Comp Neurol* 510:47–67.
- Tokuyasu KT. 1973. A technique for ultracytometry of cell suspensions and tissues. *J Cell Biol* 57:551–565.

- tom Dieck S, Brandstätter JH. 2006. Ribbon synapses of the retina. *Cell Tissue Res* 326:339–346.
- tom Dieck S, Specht D, Strenzke N, Hida Y, Krishnamoorthy V, Schmidt KF, Inoue E, Ishizaki H, Tanaka-Okamoto M, Miyoshi J, Hagiwara A, Brandstätter JH, Lowel S, Gollisch T, Ohtsuka T, Moser T. 2012. Deletion of the presynaptic scaffold CAST reduces active zone size in rod photoreceptors and impairs visual processing. *J Neurosci* 32:12192–12203.
- Vessey KA, Greferath U, Jobling AI, Phipps JA, Ho T, Waugh M, Fletcher EL. 2012. Ccl2/Cx3cr1 knockout mice have inner retinal dysfunction but are not an accelerated model of AMD. *Invest Ophthalmol Vis Sci* 53:7833–7846.
- Vistamehr S, Tian N. 2004. Light deprivation suppresses the light response of inner retina in both young and adult mouse. *Vis Neurosci* 21:23–37.
- Wahlin KJ, Moreira EF, Huang H, Yu N, Adler R. 2008. Molecular dynamics of photoreceptor synapse formation in the developing chick retina. *J Comp Neurol* 506:822–837.
- Wahlin KJ, Hackler L Jr, Adler R, Zack DJ. 2010. Alternative splicing of neuroligin and its protein distribution in the outer plexiform layer of the chicken retina. *J Comp Neurol* 518:4938–4962.
- Watabe K, Ito A, Koma YI, Kitamura Y. 2003. IGSF4: a new intercellular adhesion molecule that is called by three names, TSLC1, SglGSF and SynCAM, by virtue of its diverse function. *Histol Histopathol* 18:1321–1329.
- West MJ, Slomianka L, Gundersen HJ. 1991. Unbiased stereological estimation of the total number of neurons in the subdivisions of the rat hippocampus using the optical fractionator. *Anat Rec* 231:482–497.
- Weymouth AE, Vingrys AJ. 2008. Rodent electroretinography: methods for extraction and interpretation of rod and cone responses. *Progr Ret Eye Res* 27:1–44.
- Witkovsky P, Dudek FE, Ripps H. 1975. Slow PIII component of the carp electroretinogram. *J Gen Physiol* 65:119–134.
- Yamagata M, Sanes JR. 2008. Dscam and Sidekick proteins direct lamina-specific synaptic connections in vertebrate retina. *Nature* 451:465–469.
- Yamagata M, Sanes JR. 2012. Expanding the Ig superfamily code for laminar specificity in retina: expression and role of contactins. *J Neurosci* 32:14402–14414.
- Yang J, Pawlyk B, Wen XH, Adamian M, Soloviev M, Michaud N, Zhao Y, Sandberg MA, Makino CL, Li T. 2007. Mpp4 is required for proper localization of plasma membrane calcium ATPases and maintenance of calcium homeostasis at the rod photoreceptor synaptic terminals. *Hum Mol Genet* 16:1017–1029.
- Yen LH, Sibley JT, Constantine-Paton M. 1993. Fine-structural alterations and clustering of developing synapses after chronic treatments with low levels of NMDA. *J Neurosci* 13:4949–4960.
- Zenisek D, Horst NK, Merrifield C, Sterling P, Matthews G. 2004. Visualizing synaptic ribbons in the living cell. *J Neurosci* 24:9752–9759.
- Zhang H, Li S, Doan T, Rieke F, Detwiler PB, Frederick JM, Baehr W. 2007. Deletion of PrBP/delta impedes transport of GRK1 and PDE6 catalytic subunits to photoreceptor outer segments. *Proc Natl Acad Sci U S A* 104:8857–8862.